Journal of Power Sources 562 (2023) 232734

Contents lists available at ScienceDirect

Journal of Power Sources

journal homepage: www.elsevier.com/locate/jpowsour

Review article

Recent advancements in high performance polymer electrolyte fuel cell electrode fabrication – Novel materials and manufacturing processes

M. Grandi [a,1], S. Rohde [b,1], D.J. Liu [c], B. Gollas [b], V. Hacker [a,*]

[a] Institute of Chemical Engineering and Environmental Technology, Graz University of Technology, Inffeldgasse 25/C, 8010, Graz, Austria
[b] Institute for Chemistry and Technology of Materials, Graz University of Technology, Stremayrgasse 9, 8010, Graz, Austria
[c] Chemical Sciences and Engineering Division, Argonne National Laboratory, Lemont, IL, 60439, USA

HIGHLIGHTS

- Standardized comparison of materials and manufacturing processes.
- Recent advances in novel catalysts, catalyst support materials and ionomers for PEFC.
- Evaluation of the impact of materials and fabrication on fuel cell performance.

ABSTRACT

The global effort to introduce polymer electrolyte fuel cells for clean and renewable energy to the market is increasing the demand for high performance, robust and affordable membrane electrode assemblies (MEAs). There is not yet a standard method for large scale production of MEAs, or the methods employed are generally unsatisfactory in terms of quality and performance. A large number of published data of newly developed catalyst and electrolyte materials, claim to improve the state of the art, but are often not fully comparable due to different experimental studies and experimental designs.

This article summarizes the trends in material developments and emerging MEA-manufacturing techniques. The materials and techniques are systematically compared in terms of cell performance and scalability. Current and future scientific challenges are identified and analysed based on published findings over the past five years. Finally, the results of the cited papers have been quantitatively compared to each other and to the internal benchmarks used in each cited work to provide a complete picture of the state of the art in PEFC MEA manufacturing.

1. Introduction

Fuel cell technology is being considered one of the promising ways to enable the transition to a fossil fuel independent future [1,2]. In particular, polymer electrolyte fuel cells (PEFCs) are of high interest due to their low operating temperature, high power density and potential scalability. The electrochemical energy conversion reactions, in which the fuel hydrogen is oxidized with atmospheric oxygen and converted into water, electricity and heat, occur on platinum or platinum group metal surfaces within the catalyst layer of the membrane electrode assembly (MEA). Hence, the MEA can be considered the heart of a fuel cell, and much of recent fuel cell research focuses on its optimization. The MEA consists of a polymer membrane electrolyte sandwiched by an anode where hydrogen is oxidized through the hydrogen oxidation reaction (HOR) and a cathode where the oxygen is reduced through the oxygen reduction reaction (ORR). The electrodes are a significant cost factor in the construction of PEFC systems. This is also shown by cost projections conducted by the U.S Department of Energy (DOE) in 2004, 2005, and 2017 [3,4]. In the decade between the two studies, the absolute cost of an 80 kW PEFC stack more than halved from $ 108 to $ 45 per kW. In all three scenarios, the cost share of the electrodes in the stack is always above 30% even if an increase in performance and a significant reduction of the projected platinum loading from 0.3 to 0.125 mg cm^{-2} and a mass production of fuel cell stacks are considered. This is presumably due to the high cost of platinum. In fact, the price of platinum is highly volatile, dependent on mining practices as well as social and geopolitical uncertainties [5] and will likely rise in the long term. Furthermore, sudden platinum price increases affect the cost share of the electrode. Catalyst loading and power density of the studied baseline system were both increased between 2004 and 2005 to better represent the state of the art at that time. This increase slightly increased the cost share distribution. However the highest increase in the share resulted

* Corresponding author.
E-mail address: viktor.hacker@tugraz.at (V. Hacker).
[1] These authors contributed equally.

https://doi.org/10.1016/j.jpowsour.2023.232734
Received 2 June 2022; Received in revised form 16 January 2023; Accepted 20 January 2023
Available online 11 February 2023

from the price increase of platinum from 450 to 900 $/troz [3,4]. Hence, in order to reduce overall manufacturing costs, the platinum content needs to be reduced even further, while at the same time the power density must be increased [3,6,7]. It is anticipated that these cost factors will be further amplified as soon as production rates ramp up due to the economy of scale. The objective of this review is to build upon lessons learned from previous literature [8–10] and to describe and analyse recent advancements in applied science that have been made in the optimization of PEFC electrodes and MEAs, with a focus on performance enhancement and platinum loading reduction.

Multiple approaches can be applied to improve MEA performance at lower cost. A well-known way to achieve lower platinum loadings has been to use platinum alloys (or platinum group metals, PGMs) with inexpensive metals to create novel catalysts with even improved activity [11]. Another way is to adopt new ionic conducting polymeric binders (ionomer) during electrode fabrication to increase platinum usage. There have been many improvements recently in novel ionomers, which have superior properties compared to conventional Nafion^{TM}. Complementary to material development and optimization, attempts are made to efficiently use all catalyst particles available in the electrode with innovative electrode fabrication methods. This can be achieved through increased surface contact between the catalytically active sites, and the gaseous reactants through optimization of the "triple phase boundary (TPB)" where proton, electron and gas molecules meet [12,13] leading to optimal gas transport to the active sites and excellent electrical conductivity during fuel cell operation [14–18].

This review article is organized in five sections. Section 1 provides a brief introduction, Section 2 discusses and summarizes novel materials like catalysts, catalyst supports, and ionomers, while Section 3 focuses on new electrode fabrication methods. In Section 4 the advancements in performance will be compared in a standardized manner. An emphasis was put onto PEMFC power density ($W \bullet cm^{-2}$) and platinum utilization ($W \bullet mg_{Pt}^{-1}$) for a given platinum loading. The findings of this review are summarized in the conclusion in Section 5.

Despite multiple efforts to standardize test procedures and hardware, the reported results from different research groups still differ significantly. Therefore, this review focuses on larger performance trends and tries to avoid over-interpretation of smaller differences. Furthermore, we assume that operating conditions and hardware matching (GDL, gaskets and bipolar plate) have been optimized to a certain degree in the cited studies.

With the aim for a combined effort to determine the current state of the art in the manufacturing of membrane electrode assemblies and identify future challenges, the Technology Collaboration Programme on Advanced Fuel Cells (AFC TCP) of the International Energy Agency held the topical meeting on 'Potential for cost reduction and performance improvement for PEFC at component and system level' at Graz University of Technology in November 2021, based on which this review article was written.

2. Novel materials for PEFC electrodes

In this section, recent improvements in the field of PEFC catalysts and ionomers and related topics are discussed. Relevant concepts are presented and briefly summarized. A performance analysis of the discussed references is provided in section 4.

2.1. Catalysts

The electrocatalysts in the fuel cell are arguably the most important component of the electrode. The electrocatalytic reactions occur on the metal surface of the catalyst. Despite its high cost, platinum is by far the most used catalyst material because it can effectively catalyse both the oxygen reduction reaction (ORR) and the hydrogen oxidation reaction (HOR). To reduce material costs in fuel cell production, international research efforts have focused on the development of catalysts with reduced or no platinum content with many types of materials and preparation methods.

In this chapter, we will very briefly describe the catalyst types that have already been tested *in situ* inside complete assembled cells and reached relevant performances to allow for a better analysis in later chapters. For the sake of focus, comparability and better understanding only materials synthesized by wet chemical methods and subsequent thermal treatments and that have been processed to CCMs with the discussed electrode manufacturing methods are compared. This excludes materials like nanostructured thin films prepared by physical vapour deposition (PVD), although they are attractive materials for future fuel cell research [19]. The parameters that were defined to determine and compare the activity of platinum based ORR catalysts designed for PEFCs are the mass activity in $A \bullet mgPt^{-1}$ and specific activity in $mA \bullet cm_{ECSA}^{-2}$, measured at 0.9 $V_{iR\text{-}free}$ vs. RHE [20]. Note that although these were intended for in-situ characterisation in complete fuel cells, they are also commonly used for ex-situ studies on the RDE. In Fig. 1 a historical overview on the development of activities can be seen. ORR catalysts that have been successfully used in MEAs are mostly simple carbon supported Pt and bimetallic PtCo, PtNi and PtCu nanoparticles. They can be divided into high-amorphous de-alloyed catalysts and shape-controlled catalysts.

De-alloyed catalysts are generally prepared by leaching the non-PGM transition metal component of the binary catalyst system after co-deposition, or by galvanic displacement reactions. The leaching results in an alloy core and a pure platinum shell. Due to lattice strain and d-band interactions between the two metals, the binding energy of oxygen and its reduction products are changed to more favourable values and the activity is increased compared to pure platinum. An alternative way of manufacturing de-alloyed catalysts is by using galvanic displacement of a pre-deposited less noble metal like Ni or Cu by a platinum salt [21–28]. The platinum cation is reduced by the Cu or Ni and forms a platinum-rich over layer and an alloy core after thermal annealing. A leaching step is used to form a shell of pure platinum

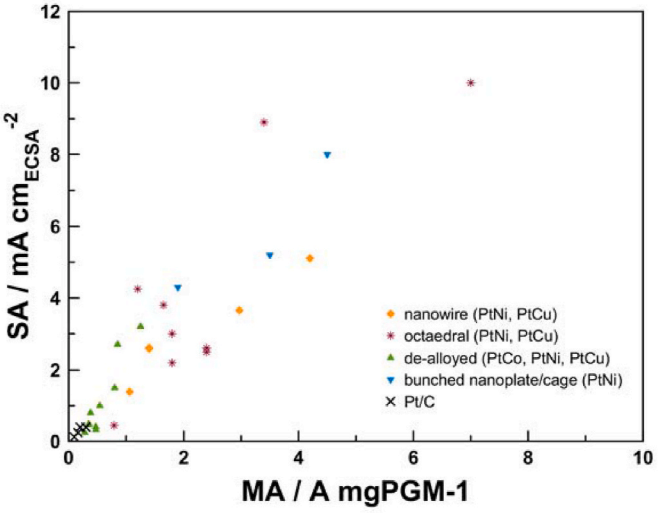

Fig. 1. Surface and mass activity of bi- and trimetallic ORR catalysts measured on a rotating disc electrode (RDE).
Platinum on carbon in black (Data extracted from Refs. [32,34,44,45]), De-alloyed catalysts in green (Data extracted from Refs. [44,46–48]), octahedral shape-controlled in red (Data extracted from Refs. [27,34–36,38,44,49,50], nanowire shape-controlled in yellow (Data extracted from Refs. [51,52]), nanoplate/cage shape controlled in blue (data extracted from Refs. [32,53]). (Measurement conditions: 0.1 M O_2-saturated $HClO_4$. ECSA for SA was determined by HUPD in N_2 saturated electrolyte except for references [36,49,50] where CO-stripping was applied.). (For interpretation of the references to colour in this figure legend, the reader is referred to the Web version of this article.)

around the core.

Shape-controlled catalyst preparation involves precise control of the crystal growth by temperature, pressure, the ratio of platinum to alloying metal (most commonly Ni) and the use of surfactants or platinum counter ions like acetyl acetonate, oleic acid, oleylamine, carbon monoxide or bromide [16,29–31] that control the growth of the particle to the desired shape. With post treatments like acid leaching, platinum skeletons with complex forms like nanocages can be obtained [32]. The principle behind these shape-controlled catalysts is to maximize the crystal planes with the highest activity, for example PtNi(111), to obtain a very high surface activity [31]. The shapes that have been synthesized range from simply increasing the level of ordering in spherical and usually more amorphous particles [22,27] to precisely obtain octahedra [33–38], hexagonal nanosheets, nanowires and nanocages [16,29–32].

PGM-free single atom catalysts for ORR are a very attractive material and there has been a substantial effort in recent years in developing platinum-group-metal-free (PGM-free) catalysts for fuel cell application [39]. They are mainly prepared by pyrolysis at high temperatures (950–1100 °C) of Fe-containing metal organic frameworks (MOF) to obtain nitrogen coordinated iron embedded in a carbon sheet structure, denoted as Fe-N-C [40–43]. A common precursor used for preparation is Fe-containing Zn-based zeolitic imidazolate framework [40,42]. Fe-N-C catalysts recently have been reported to reach comparable performance to platinum based catalysts in terms of maximum power density and show very high potential in reducing platinum content [40–43]. Since they are inherently less active for ORR they use high loadings between 4 and 6 $mg_{catalyst}$ cm^{-2} [40] yet still remain resource efficient in comparison to Pt-based catalysts. A comparison with the latter in terms of mass activity and surface activity measured on the RDE is therefore not very practical. They are therefore compared later in Section 4.1.1 based on single cell performance.

De-alloyed bi- and trimetallic Pt nanoparticles, whose development started in the early 2000s, were the first very promising catalyst materials with high activity and stability compared to Pt/C [48,54]. PtCo is the most prominent combination in this group as it is used in the Toyota Mirai's fuel cell stack [55]. They are usually prepared by co-deposition of platinum and the alloy partner, followed by a leaching step to remove the non-PGM transition metals (Co, Ni or Cu). Since the first reported activities of 0.5–0.8 $mA \bullet cm_{ECSA}^{-2}$ and 0.3–0.4 $A \bullet mg_{Pt}^{-1}$ [46,48], no relevant increase in activity was achieved. Recently prepared Pt_3Co/C reached 1 $mA \bullet cm_{ECSA}^{-2}$ and 0.54 $A \bullet mg_{Pt}^{-1}$ [56], which is still considerably lower than the high activities of shape controlled catalysts. The great advantage of these catalysts over the shape-controlled catalysts, however, are their simpler and more scalable synthesis methods. PtCu prepared by galvanic displacement was synthesized with or without controlling the crystallite growth and ordering [22,23,25,27]. It was shown by *Gatalo* et al. [27] that a double passivation method involving CO during the galvanic displacement of the precursor metal increases the surface activity compared to methods without the use of capping agents [47]. This increase was attributed to a higher degree of crystallite ordering that increases the activity towards values typical for shape-controlled catalysts.

Shape controlled catalysts achieved the highest activities in RDE experiments [36,45,52,53,57–59]. For example, octahedral Pt_3Ni/C [36,59] reached mass activities of 1.8 and 1.65 $A \bullet mg_{Pt}^{-1}$ at 0.9 $V_{iR\text{-}free}$ vs. RHE [36,59]. It was further shown by Huang et al., that doping of these octahedral platinum-nickel particles with molybdenum increases mass activity by more than three times. A record mass activity of 6.98 $A \bullet mg_{Pt}^{-1}$ was reached. However, the *Strasser* group was unable to reproduce this record mass activity and, based on their results [35], they doubt the beneficial effect of Mo-doping. In-contrast, the non-doped Pt_3Ni octahedral particles prepared by *Strasser* et al. [35] reached 1 $A \bullet mg_{Pt}^{-1}$ and after adding benzoic acid during the synthesis (as was done by Huang in all their catalyst preparations) the activity increased to 2 $A \bullet mg_{Pt}^{-1}$. This is in good agreement with the results obtained by Huang et al. [35] without Mo-doping (1.8 $A \bullet mg_{Pt}^{-1}$). Shape controlled particles can also be prepared with copper, as for example octahedral PtCu/C, which reached 1.2 $A \bullet mg_{Pt}^{-1}$ and 4.25 $mA \bullet cm_{ECSA}^{-2}$ and higher stability with voltage cycling compared to state of the art Pt/C [50]. The stability of PtCu could be further increased by doping the particles with gold during the synthesis [50,60,61]. Although the mass- and specific activity of the octahedral PtCu particles was reduced (still higher then Pt/C), the cycle stability was drastically increased compared to the un-doped PtCu [50].

When using bimetallic materials, it has been shown that the dissolution of the less noble metal into the polymer electrolyte material can be a critical issue for performance and lifetime of the MEA [62]. In the specific case, Nickel contaminations in the electrolyte were found to be responsible for low performance when PtNi was used without pre-leaching the catalyst. This complex pre-leaching is typically done by a thermal annealing treatment combined with strong acids to form a platinum over layer and an alloy core [24,49,63,64]. If this is not done the nickel ions can leach out during operation and displace the protons in the PFSA and lower the conductivity. Similarly *Frühwirth* et al. [65] recently presented a holistic model on the degradation of PFSA materials that shows how Fe^{2+}, Co^{2+} and Ti^{2+} can drastically increase the concentration of oxygen radicals from the Fenton reaction of hydrogen peroxide formed at OCV, one of the major culprits for chemical PFSA degradation [66]. These studies show that care should be taken, when using bi- or trimetallic catalysts in the PEFC. Very similar stability issues are found for PGM-free single atom [40–42,67] catalysts achieving high activities without the necessity of non-PGM transition metals, could increase performance without impacting lifetime of PEFCs. Alternatively, the use of $Ce^{3+/4+}$ or Ta-TiO_x as radical scavenger can be studied as mitigating strategy for the negative effects of the transition metals [67–69]. Another solution could be the application of Ni, Fe, and Co-containing materials in systems with very constant loads such as stationary and semi-stationary applications with no or little start-up and shut-down cycles. This is because the main driving forces for platinum and transition metal leaching are quick successions of load steps at high humidity [70] and hydrogen peroxide is mainly formed at OCV [66].

2.2. Catalyst support

It is well known that the most common support materials for the catalytic particles in the PEFC are amorphous carbon materials and the most well-known are commercialized under the name Vulcan XC32 (Vul), Acetylene black (AB) and Ketjen black (KB) [17,71–76]. They are the optimal materials for their high electrical conductivity, decent corrosion resistance and distinguishable by surface areas contributed by meso- ($d > 8$ nm) and microporous ($d < 2$ nm) volume [73,75]. According to the above cited references by *Kumar* et al. and *Yarlagadda* et al. Ketjen black possesses the highest surface area of 473 m^2 g^{-1} compared to Acetylene Black with 457 m^2 g^{-1} and Vulcan with 222 m^2 g^{-1}, due to its very high micropore volume. Vulcan XC 32 in contrast has a very low micropore volume and higher mesoporosity. These structural differences lead to a large discrepancy in the catalyst performance in the fuel cell. This different pore structure is schematically represented in Fig. 2 (a). The pore structure significantly influences how the ionomer covers the metal particles and at which humidification level the particles are in electrolyte contact. Especially for microporous carbon, sufficiently high levels of gas humidification are required to contact all outer- and inner metal particles with the electrolyte and activate them as depicted in Fig. 2 (a). This also means that at high humidification levels, gases have to diffuse through water filled pores, which affects high current density behaviour [72–74].

A second important characteristic of these carbons is the tendency to form agglomerates (1–10 μm) and clusters or fractal aggregates (100–200 nm) in a dispersion, which need to be broken up as much as possible to the single particles (10–30 nm). During catalyst preparation and active layer deposition processes the degree of the agglomerate/cluster dispersion has a significant influence on the distribution of the catalytic particles and the ionomer and in consequence final

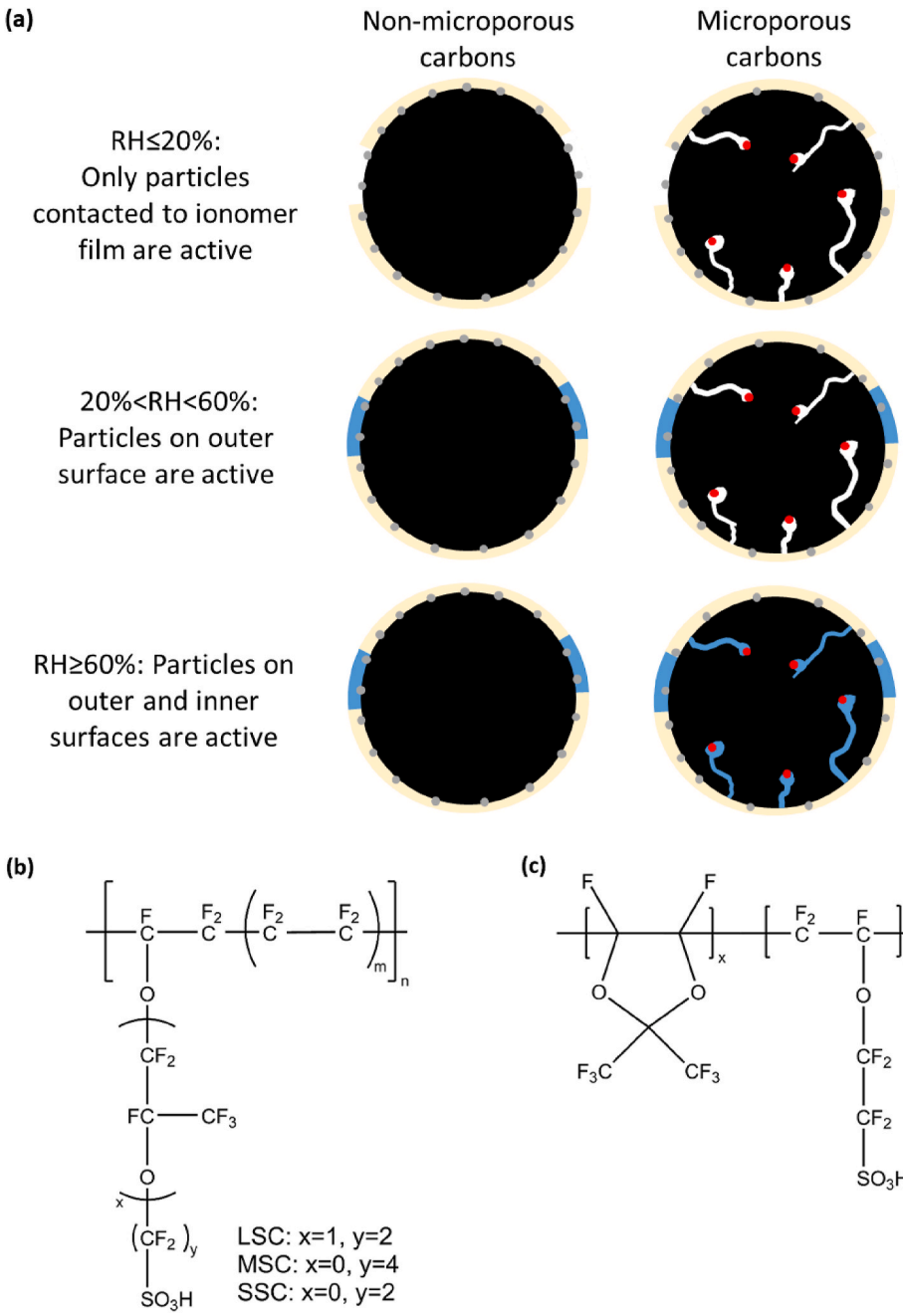

Fig. 2. Schematic representation of different carbon types their pore structures and model of liquid water localisation with various humidification stages. Redrawn with permission (CC by 4.0) from Ref. [72] (a). Condensed water is represented in blue, outer metal particles in grey, inner metal particles in red and the discontinuous ionomer film in light yellow. Typical chemical structure of PFSA ionomers reproduced from literature [14,18] (b–c). Long side chain ionomers (LSCI) were the first commercialized ionomers and possess long and flexible side chains, while medium- and short side chain (MSCI and SSCI) use shorter side chains (b). High oxygen permeability ionomers include ring structures in the main chain (c). (For interpretation of the references to colour in this figure legend, the reader is referred to the Web version of this article.)

performance [17,76].

Apart from the differences in morphology and structure, the composition of the surface must be considered, especially during catalyst synthesis as oxygen, sulphur and nitrogen can be found in varying amount depending on previous treatments [71]. These surface functionalities not only influence the dispersibility in polar solvents and water but act as starting points for metal particle growth. Since the precursors for platinum and transition metal deposition are ionic species ($PtCl_6^{2-}$, $PtCl_4^{2-}$, $Ni^{2/3+}$, $Co^{2/3+}$ and $Cu^{2/3+}$) they tend to adsorb at the polar surface functionalities [71].

Finally, the carbon containing intrinsic catalytic activity is also being explored as the supports in fuel cell application. For example, PGM-free ORR catalysts derived from the heat-activated cobalt metal organic frameworks have been used as the support to prepare PtCo core-shell catalyst [77]. The resulting catalyst showed an excellent ORR and fuel cell performances, presumably due to the synergistic catalysis from both PtCo alloy particles and PGM-free active site in the form of Co-N_x-C_y.

2.3. Polymer electrolyte materials

The polymer electrolyte in the PEFC is used to transport protons from the anode to the cathode. While mainly used to manufacture the membrane, they are also mixed in the catalyst layers as ionomers to ensure proton transport to the active sites and acts as a binder to hold together the catalyst particles. Ionomers typically have similar molecular structures of that membrane except with shorter polymer chain lengths. Therefore, they are typically provided as emulsified form in the alcohol/water mixture. After the ionomer/catalyst mixture is applied to the membrane and hot-pressed, the crosslinking reaction occurs so that the catalyst layer can be coated over the membrane surface. In the catalyst layer, the ionomer material must serve different roles than the polymer electrolyte used in the membrane in addition to the main task of proton

transport. While low hydrogen and oxygen permeability is required for membrane materials in order to avoid the gas cross-over between two electrodes, the role of the ionomer is to improve the ion conductivity while maintaining the maximal gas permeability between the reactant to the catalytic site on the electrodes.

A number of commercially available polymer electrolyte materials such as Nafion™ (Du-Pont), Neosepta-F™ (Tokuyama), Gore-Select™ (W.L. Gore and Associates, Inc.), Flemion™ (AGC Chemical), Asiplex™ (Asahi KASEI) and Aquivion® (Solvay) are available. These perfluorinated sulfonic acid (PFSA) ionomers are used because of their high proton conductivity and excellent chemical stability. Fig. 2(b–c) gives an overview of the common structures of PFSA ionomers described in literature. They are classified in i) long side chain (LSCI), ii) medium side chain (MSCI), iii) short side chain (SSCI) and iv) high oxygen permeability ionomers (HOPI).

The shortening of the side chains leads to higher ion exchange capacity (IEC) and water uptake and lower equivalent weight with the same mechanical properties as the long side chain (LSCI) counterparts [18,78] and thus increasing proton conductivity. Recently, high oxygen permeability ionomers (HOPI) have been developed by incorporating ring structures in the main chain of SSCI [14,79], as can be seen in Fig. 2 (b–c). The new monomer increases the free volume of the polymer because of the steric effect introduced by the bulky cyclic structure of the added monomer. This in turn increases oxygen permeability by up to 20–50% compared to commercial ionomers at full humidification without significantly affecting proton conductivity [14,79].

3. Manufacturing methods

An issue with many electrode manufacturing methods is that they produce catalyst layers with limited porosity and non-sufficient mass transport, which reduces FC performance particularly at high current densities. Furthermore, many electrode-manufacturing methods require catalyst inks (a slurry containing dispersed catalyst powder, ionomer and solvents), which often cause the platinum particles to agglomerate in solution and consequently decrease the catalytically active surface area. Another common problem of conventional electrode fabrication methods is the lack of uniformity in ionomer distribution, where some catalyst particles are fully covered in ionomer, which blocks the mass transport of reactants towards the catalyst particle, while other particles are not in contact with the ionomer at all, starving the catalyst of protons during operation [80]. These problems can be minimized by optimizing the electrode fabrication method with a focus on uniform catalyst distribution, limiting particle agglomeration, ensuring adequate ionomer coverage while maintaining a porous catalyst layer structure. A multitude of different electrode fabrication methods are discussed and reviewed in literature [81–83] and catalyst ink-based methods like spraying or printing are by far the most used electrode manufacturing processes. They work by depositing the ink either onto the gas diffusion layer to form gas diffusion electrodes (GDEs) or onto the membrane to form catalyst-coated membranes (CCMs). Other methods include sputtering, atomic layer deposition, electrochemical deposition, and dual ion beam-assisted deposition etc., where each method differs quite significantly and inherits individual benefits and disadvantages.

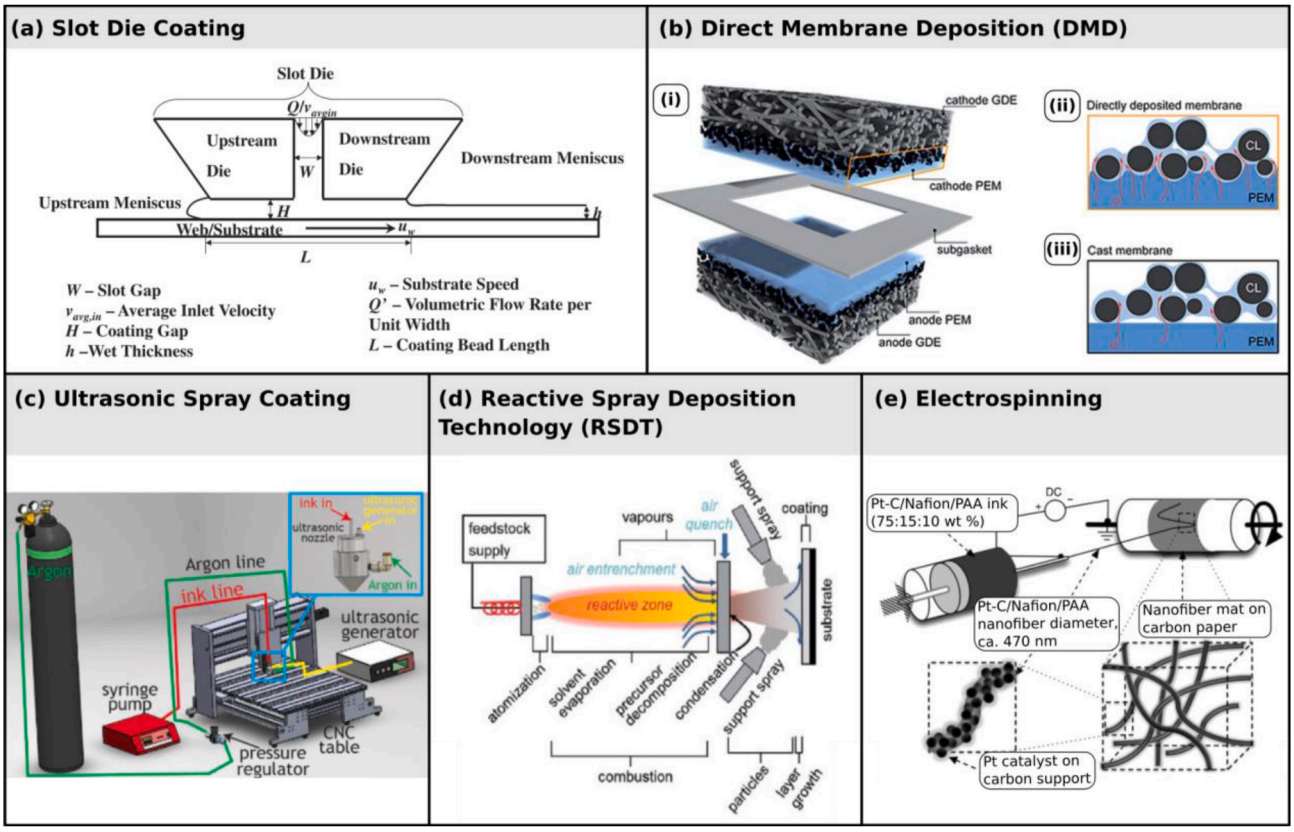

Fig. 3. (a) Schematic illustration of the slot die coating process. Reproduced from Ref. [84]. Copyright © 2013 Elsevier B.V. (b,i) Schematic depiction of the MEA construction made with direct membrane deposition. A subgasket is placed in between two GDEs to mitigate hydrogen and current crossover. (b,ii) Illustration of proton condition pathways (indicated by red arrows) from a directly deposited membrane to the catalyst layer. (b,iii) Illustration of proton condition pathways from a conventional cast membrane to the catalyst layer (Reprinted from Klingele et al. [85], CC BY 3.0). (c) Schematic drawing of the equipment used for ultrasonic spray coating. Reprinted with permission from Ref. [86]. Copyright © 2017, American Chemical Society. (d) Schematic representation of the RSDT working principle. Reproduced with permission from Ref. [87]. Copyright 2012 Elsevier. (e) Electrospinning apparatus used for catalyst layer manufacturing. (From Zhang W. and Pintauro PN. "High-performance nanofiber fuel cell electrodes". ChemSusChem 2011; 4:1753–7. 2011, Wiley-VCH Verlag GmbH& Co. KGaA, Weinheim. Reprinted with permission.). (For interpretation of the references to colour in this figure legend, the reader is referred to the Web version of this article.)

In the following sections a few selected electrode manufacturing methods are discussed, which have been investigated in recent years. A comparative overview of the extracted performance parameters of discussed references is given in Table 2 and discussed in section 4.2 while a schematic illustration of the respective working principle is given in Fig. 3.

3.1. Slot die coating

Slot die coating is a thin film coating method capable of producing catalyst layers and proton exchange membranes. It works by moving a substrate beneath the slot die through which a liquid like catalyst ink or ionomer is pumped. Hence a thin film is coated onto the substrate, and the film properties can be controlled by the flow rate, lateral motion, and distance between the substrate and slot. Detailed descriptions of the slot die coating operation can be found in literature [88] and a schematic illustration of the slot die process with its most relevant parameters is shown in Fig. 3a. Since this method can be easily integrated into industrial roll-to-roll extrusion systems, it is largely considered to be the most promising large scale MEA fabrication method because of its high scalability [89–91].

In 2010, Ding et al. [92] used the slot die extrusion process to deposit ionomer onto GDEs, followed by coating over the membrane. The substrates were carried over a heated plate to accelerate the drying process, yet no information regarding the temperature of the hot plate or the drying duration is given. The uniformity of the resulting membrane as well as the penetration and dispersion of the ionomer into the GDE were analysed by SEM and EDX measurements. A membrane was successfully deposited onto the GDE, but cracks and the non-uniformity of the catalyst layer led to an uneven membrane morphology. It was found that pre-treating the GDE by pressing it between two flat glass plates smoothens the catalyst layer, yet cracks persisted. Furthermore, they found that impediment of ionomer into the cracks can be decreased by subsequently heating the substrate, which accelerates solvent evaporation. It was shown that the penetration of Nafion™ into the catalyst layer was decreased by 40% if the substrate was heated after coating.

Building upon the knowledge gained from these preliminary coating experiments, Ding et al. [93] investigated the fabrication of fully functional MEAs. Flat and crack-free gas diffusion electrodes were prepared by hand spraying a catalyst ink slurry onto Toray 060 carbon paper and the membrane was coated on top of it using the slot die process. Subsequently, another catalyst layer was hand sprayed onto the freshly coated membrane and a second GDL was added without hot pressing. The performance of the MEA was tested in two different orientations. One where the anode side had a coated membrane and the cathode side was sprayed and the opposite orientation, where the cathode side had a coated membrane, and the anode was sprayed. Furthermore, two internal reference MEAs were made by spraying both catalyst layers and using a commercial NR-212 membrane or a membrane cast on glass. Current-voltage (I-V) polarization experiments revealed that all MEAs with slot die coated membranes performed worse compared to the two reference MEAs, which both had almost identical performance. At 0.6 V the MEA with the membrane coated onto the cathode side had a current density of 0.51 A cm^{-2}, the MEA with the membrane coated onto the anode side had a current density of 0.85 A cm^{-2} (see for Table 2 more details) while both reference MEAs had a current density of 1.08 A cm^{-2}. EIS measurements revealed that the MEA with the membrane coated onto the cathode side inherited the largest high frequency arc, pointing to a severe oxygen-transport limitation. The authors suggest incorporating a microporous layer into the MEA and accelerating the solvent evaporation directly after coating to improve the performance of the MEAs with slot die coated membranes.

In 2019, *Stähler* et al. [91] fabricated a completely coated MEA, where both catalyst layers and the membrane were made with the slot die coating process. While the focus of this work was to fabricate a PEM water electrolyser, many of the processing steps can be readily applied to manufacture PEM fuel cells, as stated in a previous publication by the same authors [94]. With their approach, they were able to deposit each layer (anode, membrane and cathode) successively on top of each other using only one tool, which drastically simplifies the manufacturing process and improves scalability.

Unfortunately, there is only a limited number of accessible publications applying the slot die coating process to manufacture conventional PEFCs, with most of the openly available research focusing on high temperature PEFCs [89,90,95,96].

3.2. Ultrasonic spray coating

Ultrasonic spray coating is an improvement of the conventional hand spraying technique. An ultrasonic nozzle is incorporated into the spray gun, which is usually not operated by hand but with an automatic apparatus as shown in Fig. 3c. This yields a higher dispersion of the catalyst particles in the ink and both CCMs and GDEs can be produced by this method in a reliable and reproducible manner.

Millington et al. [97] were the first to describe this method and they compared a conventional hand spray method to this ultrasonic method by using a Sono-Tek Ultrasonic Spray system. The catalyst ink is pumped through the vibrating nozzle where it is dispersed into a fine mist and an inert gas like argon is used to carry the components. The authors deposited the catalyst layer on top of five different commercially available gas diffusion layers to fabricate GDEs. Three different loadings were prepared and the GDEs were subsequently dried at 50 °C. The authors claim that the ultrasonic method leads to a de-agglomeration of platinum particles since micron size droplets are formed in the process. Hence, higher performing fuel cells can be made, and the effect is particularly pronounced at lower catalyst loadings. This claim is backed by the observation that fuel cells with ultrasonically produced catalyst layers performed better than fuel cells, which were produced with the conventional hand spraying method. This effect was notably pronounced at low Pt loadings of 0.15 and 0.05 mg cm^{-2}, while at a higher loading of 0.4 mg cm^{-2} both fuel cells performed similarly.

Sassin et al. [86] gave a detailed description, list of materials and precise procedure to manufacture CCM membrane electrode assemblies with the ultrasonic spray coating technique. Additionally, a heated vacuum plate (80°–90 °C) is placed beneath the nozzle and the PEM is held on top of it to accelerate the evaporation of solvents. A key advantage of the ultrasonic deposition method is its reproducibility, since the deposition velocity, pattern and nozzle height are automatically controlled. By achieving a unitized approach to this method and clearly defining its parameters, researchers could gain more confidence in their data and a meaningful comparison of different results is facilitated. Finally, the authors highlighted that post-deposition processing strongly affects the overall fuel cell performance. For example, over-compression damages the pore structure and thus limits the mass transport, while insufficient compression increases the ohmic resistance of the cell.

Recently, Kabir et al. [98] compared the performance of ultrasonically sprayed electrodes to electro-spun electrodes (see chapter 3.4). It is remarkable that even though the published results of the ultrasonic process are very good in comparison to the results of other ultrasonic publications, the performance is still inferior in comparison to the electrospinning process. The fuel cell with ultrasonically produced electrodes was outperformed especially at high current densities (>1 A cm^2). It is suggested that the large inter-fibre voids of the electrospun nanofibers lead to a much better gas transport and water removal in comparison to the ultrasonic process (see section 3.4).

3.3. Reactive spray deposition technology (RSDT)

Reactive spray deposition technology is a flame-based catalyst

synthesis method, which is capable of directly depositing freshly synthesized catalyst particles onto a PEM or other substrates. It is a promising method to cost effectively fabricate MEAs, because all steps related to catalyst fabrication and deposition are harmonized into one processing step. A scheme describing the working principle of this method is shown in Fig. 3d.

The method starts by creating a precursor solution with the desired elemental composition of the catalyst. The solution is subsequently pumped through a needle, atomized, and ignited creating the RSDT flame, which is controlled and stabilized with an oxygen/methane mix. After the flame, an air quench is installed to cool down the mixture. Additional secondary nozzles can be installed to add components like the catalyst support or ionomer. Hence, many parameters influencing the catalyst layer formation are individually controllable without the need of an intermingled catalyst slurry. Furthermore, the air quench cools the mixtures sufficiently for the catalyst to be deposited directly onto the PEM.

Yu et al. [99] studied the influence of the inonomer/carbon ratio onto the microstructure formation of the catalyst layer and the overall PEFC performance. The Pt nanoparticles were deposited onto the PEM and Vulcan XC-72R was used as the catalyst support. Mercury porosimetry, nitrogen adsorption and SEM were used to investigate the catalyst layer (CL) microstructure. A bimodal pore size distribution was found with primary-pore diameters ranging from 1.7 nm to 10 nm and those of secondary-pores ranging from 30 nm to 100 nm. While the choice of catalyst support material is the most important parameter defining the CL microstructure [100,101], also the ionomer coverage is of key importance since it directly influences the PEFC performance by facilitating proton transport to Pt particles in obscured locations like micro-pores. The authors found that CLs fabricated with the RSDT method showed surface areas and pore size distributions similar to CLs fabricated with conventional spraying or decal methods. However, a single cell test revealed that the best electrochemical performance was reached at a ionomer/carbon ratio of 0.3, which is lower than that in conventional methods. Moreover, a high in-situ ECSA value of 62 $m^2 g_{Pt}^{-1}$ was determined in the fuel cell, which indicates a better Pt utilization. Thus, the authors claim that the RSDT process facilitates ionomer coverage even inside the primary pores, which are usually too small for ionomer coverage. This behaviour could be explained by the premixing of ionomer and carbon prior to catalyst deposition, which helps the ionomer to better cover the carbon particles.

In a follow-up paper published by Yu et al. [102], several CCMs were fabricated using the RSDT process to investigate the properties of three different support materials namely Ketjen Black, multi-wall carbon nanotubes and reduced graphene oxide. The deposited catalyst layers were investigated ex-situ by RDE experiments as well as in-situ to determine the overall PEFC performance. Transmission electron microscopy revealed that the average size of the Pt nanoparticles was 2.0–2.2 nm in Ketjen Black and the reduced graphene oxide. The Pt particles on the multi-wall carbon nanotubes support were slightly bigger with 2.5 nm and they were more agglomerated. The RDE data revealed that the catalyst layer with Ketjen Black had the highest ECSA (127,1 $m^2 g_{Pt}^{-1}$) of the tested catalyst supports. Furthermore, the measured mass activity of 0.4 $A mg_{Pt}^{-1}$ and specific activity of 315 $\mu A\ cm_{Pt}^{-2}$ of the catalyst layer with Ketjen Black was twice as high as the reported commercial values [103]. Finally, the authors successfully manufactured MEAs with ultra-low Pt loadings with all three catalyst support materials and the PEFC with Ketjen Black showed the best performance.

Finally, Yu et al. [104] use RSDT to fabricate a graded catalyst layer which is discussed in mor detail in Section 3.5. The performance of all RSDT MEAs discussed in this review is summarized in Table 2.

3.4. Electrospinning

Electrospinning is a well-established method to produce nanometre sized fibres with a given diameter, a defined axial ratio and lengths, which can approach infinity [105]. A wide variety of different materials has been successfully utilized to produce nanofibers with this method including metals, ceramics, glasses, and polymers. This process works by creating a solution, suspension or melt of the envisaged material, which is subsequently pumped through a syringe with an inner needle diameter of a few micrometres (the die). An electric field is generated by applying a high voltage between the needle and the counter electrode, tearing the droplet at the needle tip into fibrous form as it accelerates towards the counter electrode in a nanometre-sized jet. However, the jet does not travel in a linear motion on its path towards the counter electrode, yet it bends in a complicated but not random spiralling trajectory. Certain self-assembly processes driven by the Coulomb repulsion of charged particles in the liquid cause these so-called bending instabilities, which have been discussed in detail elsewhere [105,106]. This phenomenon can be predicted theoretically and controlled experimentally and thus a wide variety of different nanofiber architectures can be fabricated like fibres with spherical beads, twisted fibres, cross grating fibres and fibres in zigzag arrangements.

For the use in PEM fuel cells, electrospinning has been employed to produce catalyst supports [107–111] and Nafion™-based proton exchange membranes [112,113], which can be used as alternatives to conventional carbon black catalyst support and thin film Nafion™ membranes.

In 2009, *Kotera* et al. [114] were the first to describe how PEFC electrodes can be manufactured by electrospinning. With this method a nanometre mesh with exceptional gas diffusion properties due to its large inter-fibre voids is deposited onto the counter electrode. Since then, several publications from different groups were released and different aspects of this process were evaluated, discussed, and improved. A review summarizing this research topic was published recently by Waldrop et al. [115].

To produce nanofiber electrodes, the counter electrode consists of a rotating and horizontally oscillating cylinder, which collects the incoming stream of nanofibers, as it can be seen in the schematic drawing of this process in Fig. 3e. Furthermore, the fibres can be deposited directly onto substrates like carbon paper mounted onto the rotating cylinder. The platinum/catalyst loading is controlled by varying the deposition duration.

In contrast to conventional MEA production catalyst inks, which consist of a solvent (e.g. water and isopropanol), ionomer (e.g. perfluorosulfonic acid, PFSA) and the dispersed catalyst powder, the electrospinning ink requires an additional carrier polymer. This needs to be added to give the dispersion enough stability to endure the electrospinning process. Poly (ethylene oxide) (PEO) or poly (acrylic acid) (PAA) have been used as carrier polymers, since PFSA on its own has an insufficient number of polymer chain entanglements and thus insufficient stability for the spinning process [116]. Additionally, the rapid stretching of the ejected ink on its trajectory towards the counter electrode leads to strong shear forces within the jet, and it is assumed that this might lead to a disaggregation of nanoparticles [115].

Kotera et al. [114] were the first to publish results of electro-spun electrodes for PEFCs with catalytically active nanofibers using a double co-axial channel nozzle. The catalyst ink solution consisting of Flemion™, a catalyst dispersion and solvents was fed through an inner needle opening and a 0.3 wt% PEO solution was fed through the outer sheath. The resulting fibre electrode had a catalyst ink core supported by an outer PEO layer. The deposited nanofiber mesh had an in-plane gas permeability ten times higher than the in-house slurry coated electrodes. Additionally, the fuel cell with electro-spun electrodes showed better performance at higher current densities compared to the in-house standard. The authors contributed this increased performance to beneficial mass transfer properties arising from the porous nature of

inter-fibre voids in the electro-spun electrode.

In 2011, *Zhang & Pintauro* [117] reported the first electro spun nanofiber electrodes using a single channel nozzle without the need of a core-sheath setup, further simplifying the process. In a series of follow up articles [118–123], they discussed many details of this process. The initial publication of this group explains how the carrier polymer PAA was mixed directly into a dispersion of Pt/C catalyst powder, isopropanol, and water with dissolved perfluorosulfonic acid. This resulted in catalytically active nanofibers with an average diameter of 470 nm, which were deposited directly onto carbon paper. Hence, this method produces nanofiber GDEs, which are subsequently pressed onto a Nafion^{TM} membrane. The authors also investigated the effect of hot-pressing onto the fibre structure and found that increasing pressure and temperature reduces porosity, yet the fibre morphology is retained. The performance of the electro-spun electrodes was compared to an in-house fabricated decal electrode. An ECSA of 60 m^2g^{-1} was found for the decal electrode with a standard in-situ MEA cyclic voltammetric technique, while 114 m^2g^{-1} were found for the electro-spun electrode, a value almost twice as high. The higher ECSA was attributed to a better distribution of the catalyst particles and ionomer caused by the exceptional fibre formation process. Finally, also the durability of the fabricated electrodes was evaluated with an accelerated voltage cycling test. While the in-house decal transfer electrode lost 75% of its initial ECSA, the electro-spun electrode only lost 48% under the same conditions.

In a more recent publication from the same group [123], a conventional Pt/C as well as a PtCo/C catalyst were successfully employed to form a nanowire cathode. The network of the entangled nanofibers with incorporated catalyst particles is shown in the SEM images in Fig. 4. It was found that the surface roughness contributed to 20% and intra-fibre voids up to 30% of the overall surface area of the nanowires, which further underlines the good accessibility of the incorporated platinum particles. Furthermore, a standard metal dissolution accelerated stress test with 30,000 square wave voltage cycles was performed, where the PtCo/C catalyst nanofiber MEA only lost 8% of its initial power, while the in-house manufactured spray coated MEA lost 32%.

Recently, *Khandavalli* et al. [124] investigated the effect of the carrier polymer PAA in the catalyst ink in more detail. They found that increasing the PAA concentration also increases viscosity, which leads to a better fibre evolution. However, a PAA concentration that is too high, can result in flow instabilities and fibre defects. An overview of the PAA carrier polymer concentration and the resulting fibre morphologies is given in Fig. 5.

The performance of all electrospun MEAs discussed in this review is summarized in Table 2.

3.5. Graded catalyst layers

All publications regarding electrode manufacturing methods that have been discussed so far have in common that they produce an isotropic catalyst layer, meaning that the properties and composition of the catalyst layer are equal at all positions. However, experimental data [125–127] as well as theoretical modelling [128,129] suggest an unequal reaction rate within the catalyst layer. The altering reaction conditions within the catalyst layer result from an increased proton conductivity at the catalyst layer/membrane interface and increased mass transport close to the catalyst layer/GDL interface [126]. Thus, an adapted catalyst layer composition dependent on its positioning would be beneficial, which is being addressed with so called graded catalyst layers. In this section recent publications are highlighted which produced graded catalyst layers using different approaches as well as manufacturing methods.

Yu et al. [104] used reactive spray deposition (RSDT) to fabricate a graded cathode to addresses the problem of Pt dissolution. In particular, Pt particles which are in close proximity to the membrane/cathode interface (within 6 μm) are affected as described by several research groups [130–135]. Furthermore, it is believed that this effect becomes more prominent with smaller Pt particle sizes. Hence, the authors used the flexibility of the RSDT process to change the Pt particle size during deposition. A so-called gradient cathode (i.e. graded catalyst layer) was manufactured, where a 6–7 μm thick catalyst layer containing 5 nm Pt particles was deposited onto the membrane and another 6–7 μm thick layer containing 2 nm particles was deposited on top of the first layer. Ketjen Black was used as the catalyst support, since it showed the best performance in the previous study [102]. Two internal standards with a CL containing only 2 nm or 5 nm Pt particles were made. Afterwards, the fuel cell performance as well as the ECSA of the samples before and after an accelerated stress test designed for electro catalyst degradation were compared. At the beginning of the test (BOT), the ECSA of the gradient electrode was 71 $m^2g_{Pt}^{-1}$, which is lower than the 82 $m^2g_{Pt}^{-1}$ of the 2 nm control, but bigger than that of the 5 nm control with 35 $m^2g_{Pt}^{-1}$. However, at the end of test (EOT), the gradient electrode maintained the highest ECSA with 18 $m^2g_{Pt}^{-1}$, while the 5 nm and 2 nm control had ECSAs of 9 $m^2g_{Pt}^{-1}$ and 13 $m^2g_{Pt}^{-1}$, respectively. The current density and cell voltage (I-V) polarization curves at BOT revealed that at low current densities the fuel cell with the gradient cathode performed almost similar as the 2 nm internal reference and both were better than the 5 nm internal reference. However, at higher current densities above 600 mA cm^{-2} the gradient cathode outperformed even the reference fuel cell with the 2 nm Pt particles in the CL. Finally, at EOT, the gradient cathode performed drastically better then both internal references, supporting the gradient Pt particle approach, where larger Pt particles are closer to the membrane. This approach can be used to increase the fuel cell lifetime.

Nguyen et al. [136] tried to address problems caused by the ionomer content within the cathode catalyst layer at low gas humidification. Insufficient humidification causes low ORR kinetics [137,138],

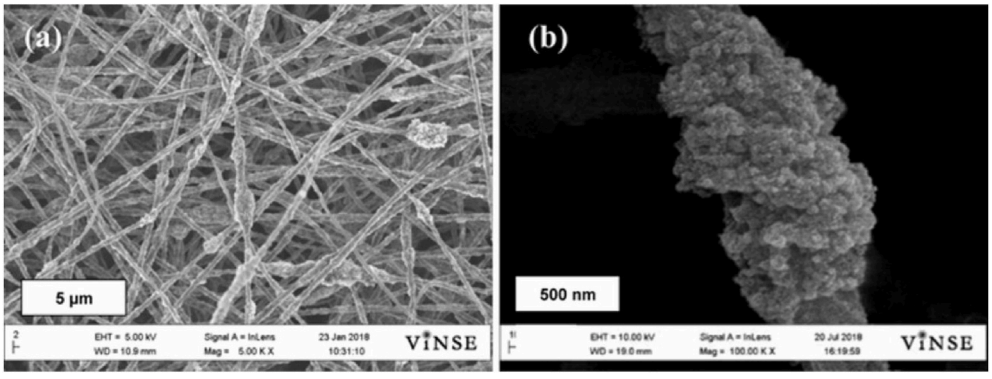

Fig. 4. SEM picture of a nanofiber mat with Nafion^{TM} and PAA binder at a magnification of (a) 5000× and a PtCo/C catalyst as well as (b) a Pt/C catalyst at a magnification of 1,00,000× (Reprinted from Slack et al. [123], CC BY 4.0).

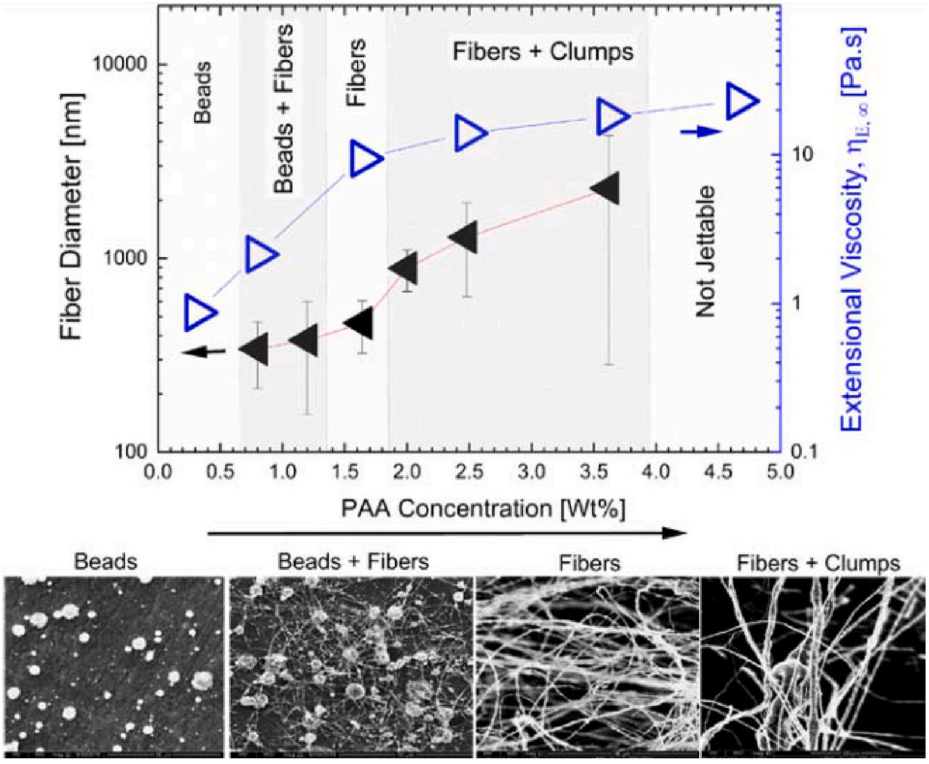

Fig. 5. Effect of PAA concentration in catalyst inks on the fibre spinnability and the resulting fibre diameter. (Reprinted with permission Khandavalli S, Sharma-Nene N, Kabir S, Sur S, Rothstein JP, Neyerlin KC et al. Toward Optimizing Electrospun Nanofiber Fuel Cell Catalyst Layers: Polymer–Particle Interactions and Spinnability. ACS Applied Polymer Materials 2021. https://doi.org/10.1021/acsapm.0c01354. Copyright 2021 American Chemical Society.)

increased oxygen transport losses [139] and an overall decreased catalyst layer utilization [128]. The authors postulated that these issues could be resolved by utilizing a graded cathode catalyst layer with a high ionomer content close to the membrane using fully-hydrocarbon-based fuel cell MEAs. Several MEAs with different ionomer to carbon rations (I/C ratio) were prepared using an ultrasonic spray coater. The best performing MEA had a I/C ratio of 0.4 in the 25% close to the membrane and I/C ratio of 0.2 at the 75% close to the GDL. These findings are in line with previous studies [126,127,140] yet they found that the impact of ionomer grading is more important for fully-hydrocarbon-based MEAs than for PFSA based MEAs. They attribute their improved performance to an increased proton conductivity at low humidity without compromising mass transport.

A double catalyst layer electrode was made by *Van Dao* et al. [141] by first spray coating a Pt/C catalyst ink onto carbon cloth and a subsequent deposition of Pt nanoparticles via electrophoresis deposition (EPD). EPD is a method to deposit Pt catalyst nanoparticles from a colloidal solution onto a conductive substrate [142–145]. This method inherits short processing times, produces a catalyst layer with good uniformity [146,147] and can aid the deposition of Pt particles near the surface of the conductive substrate to optimize catalytic sites and minimize Pt particles lost in the matrix of the electrode which improves the electrocatalytic properties [148]. However, at larger Pt-loadings Pt nanoparticles tend to agglomerate [149]. Thus, the aim of this study was to reduce the agglomeration of Pt nanoparticles by combining the EPD method with a conventional spray coating technique. Half-cell measurements revealed that the double layer electrodes had a higher ECSA and lower internal resistance than MEAs made with spray coating or EPD only, with values of 51,2 $m^2 g_{Pt}^{-1}$ vs 31,9 $m^2 g_{Pt}^{-1}$ and 34,1 $m^2 g_{Pt}^{-1}$ and 20 Ω vs 132 Ω and 120 Ω respectively. In an in-situ test the double catalyst layer electrode with a loading of 0.164 mg • cm^{-2} was used as the anode and a commercial GDE of with a loading of 0.3 mg • cm^{-2} was used as cathode. The MEA containing the double layer electrode outperformed the commercial MEA, with maximum power densities of 0.63 W • cm^{-2} at 1.12 A • cm^{-2} vs 0.32 W • cm^{-2} at 0.53 A • cm^{-2} as well as an increased Pt-utilization of 3.84 W • mg^{-1} vs 1.07 W • mg^{-1}. However, it is not quite clear to the reader why the double layer electrode is used as anode instead of the cathode with its sluggish ORR kinetics. Furthermore, additional information about the composition as well as supplier of the commercial electrode, which was used as a reference, would be beneficial.

3.6. Direct membrane deposition (DMD)

As the name suggests, direct membrane deposition is not an electrode or catalyst layer fabrication method yet a method to deposit the proton conductive membrane directly onto the catalyst layer. Impressive performances and extremely high Pt utilisations are described in literature by MEAs made with the DMD process. Hence this method is briefly introduced, even though it is no electrode fabrication method and not strictly within the focus of this section. However, to maintain the comparability of the data, the literature discussed in the following paragraphs is not included in Table 2 and the resulting discussion in Section 4.

The term “Direct membrane deposition” was coined by Klingele et al. [85] who applied drop on demand inkjet printing to print a membrane layer on top of a gas diffusion electrode. MEAs made with this method have the advantage that the contact surface area of the ionomer within the catalyst layer and the membrane layer is increased because the liquid Nafion™ dispersion penetrates the catalyst layer. Thus, a very low ionic contact resistance is achieved and an illustration of a MEA made with this method is given in Fig. 3b,i. Fig. 3b,ii symbolizes the increased number of ion conduction pathways of a deposited membrane compared to a cast membrane in Fig. 3b,iii. Using this method, the authors made a MEA with a loading of 0.5 mg • cm^{-2} at both anode and cathode that achieved power densities exceeding 4 W • cm^{-2} under

optimized conditions. Furthermore, a very low membrane ionic resistance of 12.7 $m\Omega \bullet cm^{-2}$ was measured without compromising hydrogen crossover.

In a follow-up publication Breitwieser et al. [150] made MEAs with ultra-low symmetrical Pt-loadings of 0.029 $mg \bullet cm^{-2}$. A maximum power density of 2.56 $W \bullet cm^{-2}$ was reached at fixed flow conditions with oxygen as cathodic fuel at 80 °C, 75% RH and 300 kPa(abs). This represents a peak cathodic Pt-Utilization of 88 $W \bullet mg^{-1}$ (or 44 $W \bullet mg^{-1}$ if the anode Pt content is considered as well).

Vierrath et al. [151] took a deeper look at the reasons for the improved performance of DMD fuel cells and MEAs with varying thicknesses were prepared and investigated with electrical impedance spectroscopy. Interestingly, they found that the main reason for the increased fuel cell performance is caused by an improved mass transport which accounts for 90% of the improvement.

Breitwieser et al. [152] used the DMD process in combination with electrospinning to fabricate nanocomposite fuel cell membranes by incorporating Poly (vinylidene fluoride-co-hexafluoropropylen) nanofibers into the printed membrane. In a follow-up publication nanofibers decorated with cerium oxide nanoparticles were made, which used the cerium oxide nanoparticles as radical scavengers to extend the membrane lifetime [153].

Klose et al. [154] and *Zhao* et al. [155] used the same method to make nanocomposite fuel cell membranes yet they used sulfonated poly (ether ketone) and poly (arylene ether sulfone) respectively as nanofiber material.

4. Performance analysis of different materials and manufacturing methods

As briefly mentioned before, fuel cell performance is coupled proportionally to the TPB [156,157]. Sufficient gas flux towards and from the electrodes with porous catalyst layer structures, non-agglomerating Pt particles to expose more catalytically active sites, adequate ionomer coverage at each Pt particle while maintaining a proper electrical conductivity are all critical aspects required for a high performing fuel cell. However, in practical laboratory testing scenarios also other factors like in-house manufacturing procedures and the condition of cell and testing equipment significantly influence performance results. While it is good practice to optimize laboratory conditions by comparing results to external benchmarks, we encourage not only to look at the absolute numbers, but to also acknowledge performance gains achieved against internal benchmarks. An overview over many performance parameters and operating conditions from publications discussed in this work is given in Table 1 for different materials and ink preparation methods, and in Table 2 for different electrode manufacturing methods. A fundamental parameter correlating with fuel cell performance is Pt loading, which is the amount of Pt (in milligram) contained in a square centimetre of an electrode. Higher Pt loadings increase the number of electrocatalytically active sites and lead to better performance, yet also increased cost. Note that the cathode requires a higher Pt loading than the anode due to the sluggish oxygen reduction. Another interesting parameter is the peak power density, which is the maximum power output per square centimetre of a MEA. By ensuring a sufficiently high-power density in a single MEA, the manufacturing costs can be minimized, since less cells are needed per stack. Finally, the peak Pt utilization is a crucial parameter describing the maximum power output of a fuel cell system per milligram of platinum. Higher Pt utilization values mean that less Pt is required to achieve high performing fuel cells. This is essential, since manufacturing costs can be reduced with the economy of scale, yet platinum costs always remain fixed to its market value.

4.1. In-situ and ex-situ performance of materials

4.1.1. Catalysts

In terms of platinum utilization, Fig. 6(a–b) and Table 1 show that the highest increase in platinum utilization achieved by Pt-based catalysts is by a factor of ~1.6 (compared to the platinum on carbon benchmark). It was reached by the implementation of octahedral and de-alloyed platinum-nickel into the cathode of the MEA [44]. An increase by a similar factor has been obtained with bunched nano-sheets (BNS) and nano-cages (BNC) based on the PtNi alloy [32]. However, they still did not outperform the de-alloyed catalyst type and two reasons can be identified in the relevant literature:

- Detrimental effects of the transition metal on the ionomer
- High local oxygen transport limitations or suboptimal accessibility of the catalyst particles.
- It is well known that there is a large discrepancy between ECSA, mass activity and specific

Activity measured on the RDE and in the MEA, as depicted in Fig. 7. A straightforward reason for this discrepancy is the inherently different electrolyte [16,158,159]. On the RDE, only minimal amounts of PFSA ionomer are used to ensure good dispensability of the catalyst powder and as binder in the deposited layer and perchloric acid is used as electrolyte to avoid contaminating the catalyst surface. In the MEA, the sulfonic groups of the ionomer adsorb on the catalyst and decrease its activity [16]. But this is probably not the only reason for the ECSA and activity decrease when changing from RDE to single cell. When changing the active metal from platinum to bimetallic particles, the activity is drastically increased under ex-situ conditions, as shown in Fig. 1. However, in-situ activities are not as high, because of the inherently different conditions in the MEA, as discussed in section 4.1. Particularly differences between solid and liquid electrolyte can be identified as main reasons for the lower activities. When comparing reported activities measured ex-situ and in-situ for exactly the same material by the same groups, as seen in Fig. 7, it seems that the difference between in-situ and ex-situ mass activity increases with the ex-situ determined specific activity. This could be a sign, that the highly active crystal planes such as the PtNi(111) are more susceptible to the poisoning effect of $-SO^{3-}$ than other crystal planes, since the binding energy of a molecule on the surface strongly depends on which crystal plane it is adsorbed.

The second possibility for the mismatch between in-situ and ex-situ results is inherently coupled to how the large mass activity is reached with shape-controlled nanoparticles. Since they possess extremely high specific activities, but low ECSA [31], it is crucial that no particle is blocked by any means, either by suboptimal porosity of the carbon or by large local oxygen transport limitations at the ionomer/metal interface due to strong $-SO_3^-$ adsorption. With very low oxygen concentrations at the catalyst surface, the results will not be optimal in the low and high current density region.

Additionally, to poisoning of the surface by the sulfonate groups or suboptimal oxygen accessibility, there are other constraints to performance specific only to bimetallic catalysts. It is very important to avoid any metal dissolution into the PFSA electrolyte during operation and/or manufacturing, as the ions can promote its degradation or displace the protons and lower the conductivity [62,65,160]. Leaching of the less noble metal on the particles surface has proven to greatly benefit initial performance, while destructive methods like ball milling can have adverse effects [47].

By far the largest advancement in performance by implementing new catalyst types was reached with PGM-free single atom catalysts. Table 1 and Fig. 6(a–b) show that power densities are starting to reach and in some cases surpass Pt-based CCMs, both at 0.6 V and at the maximum power point [40–43]. Only two studies however surpassed them in terms of platinum utilization in $W\ mg_{Pt}^{-1}$. One issue obstructing achievement of similarly high platinum utilisations in single cell configuration is the fact

Table 1
Fuel cell performance data using different materials extracted from polarization curves of various publications discussed in this review. The internal benchmark of each study is reported to aid comparability. To enhance comparability only results which were recorded in H2/air are shown. "n.r." = not reported.

	Year	Fabrication method	Cathode loading (Pt)	Anode loading (Pt)	Current density@0.6V	Power density @0.6V	Peak power density	Peak voltage	Peak Pt utilization	T	Back-pressure	RH	Ref.
			[mg cm^{-2}]	[mg cm^{-2}]	[A cm^{-2}]	[W cm^{-2}]	[W cm^{-2}]	[V]	[W mg_{Pt}^{-1}]	[°C]	[bar]	[%]	
Catalyst materials													
Pt/C HiSpec 4000	2019	ink jet printing	0.20	0.20	n.r.	n.r.	0.80	0.47	2.0	80	3	100	[47]
PtCu3/C leached + milled (Galvanic displacement)	2019	ink jet printing	0.20	0.20	n.r.	n.r.	0.31	0.32	0.8	80	3	100	[47]
PtCu3/C leached (Galvanic displacement)	2019	ink jet printing	0.20	0.20	1.25	0.75	0.79	0.53	2.0	80	3	100	[47]
PtNi/C Nanowires (pre-leached) Galvanic displacement 6% ionomer	2018	Ultrasonic CCM	0.13	0.25	1.55	0.93	1.00	0.55	2.6	80	0.5	100	[51]
octahedral PtNi (Mo)/C	2019	Decal	0.10	0.10	1.17	0.70	0.75	0.47	3.8	80	0.5	100	[44]
PtNi/C de-alloyed (Comm.)	2019	Decal	0.10	0.10	1.37	0.82	0.86	0.54	4.3	80	0.5	100	[44]
Pt/C 50 wt% HiSpec 8000	2019	Decal	0.20	0.20	1.50	0.90	0.98	0.49	2.5	80	0.5	100	[44]
PtNi BNC/C	2019	Spray coated	0.15	0.10	1.48	0.89	0.92	0.56	3.7	80	2	100	[32]
PtNi BNS/C	2019	Spray coated	0.15	0.10	1.04	0.26	0.77	0.48	3.1	80	2	100	[32]
Pt/C (60%)	2019	Spray coated	0.15	0.10	0.79	0.20	0.60	0.47	2.4	80	2	100	[32]
Fe-N-C	2020	Paint brush CCM	n.r.	0.2	0.36	0.22	0.38	0.41	1.9	80	0.5	100	[42]
Fe-N-C	2020	Doctor blade GDE	0[a]	0.3	0.80	0.48	0.61	0.44	2	94	0.7	80	[41]
Fe-N-C	2021	Spray coated	0[a]	0.2	0.30	0.18	0.31	0.40	1.5	80	0.5	100	[40]
Fe-N-C	2021	Spray coated	0[a]	0.035	0.30	0.18	0.31	0.40	8.8	80	0.5	100	[40]
Fe-N-MC	2022	Spray coated	0[a]	0.1	0.79	0.48	0.54	0.44	5.4	70	1	n.r.	[43]
Ink Pre-treatment													
10 s ultras. tip +20 min ultras. bath	2019	Ultrasonic CCM	0.04	0.10	0.58	0.35	0.45	0.45	3.2	80	0.5	100	[17]
10 s ultras. tip +1 min ultras. bath	2019	Ultrasonic CCM	0.04	0.10	0.40	0.24	0.43	0.43	3.1	80	0.5	100	[17]
20 min ultras. bath	2019	Ultrasonic CCM	0.04	0.10	0.58	0.35	0.45	0.45	3.2	80	0.5	100	[17]
20 min ultras. tip	2019	Ultrasonic CCM	0.04	0.10	0.49	0.29	0.42	0.42	3.0	80	0.5	100	[17]
5 min ultras. tip	2019	Ultrasonic CCM	0.04	0.10	0.40	0.24	0.38	0.38	2.7	80	0.5	100	[17]
5 min ultras. Bath	2019	Ultrasonic CCM	0.04	0.10	0.50	0.30	0.44	0.44	3.1	80	0.5	100	[17]
ODT masked 100%RH	2020	Decal	0.17	0.17	1.20	0.72	1.01	0.35	3.0	80	0.8	100	[15]
ODT masked 50%RH	2020	Decal	0.17	0.17	0.88	0.53	0.82	0.41	2.4	80	0.8	50	[15]
Unmasked, 100% RH	2020	Decal	0.17	0.17	1.20	0.72	0.64	0.40	1.9	80	0.8	100	[15]
unmasked, 50% RH	2020	Decal	0.17	0.17	0.69	0.42	0.90	0.38	2.7	80	0.8	50	[15]
Polymer electrolyte materials													
LSCI 1100 EW (Nafion)	2021	Decal	0.10	0.03	1.60	0.96	1.00	0.50	8.0	80	0.5	100	[18]
SSCI 980 EW	2021	Decal	0.10	0.03	1.77	1.06	1.11	0.55	8.9	80	0.5	100	[18]
SSCI 790 EW	2021	Decal	0.10	0.03	1.90	1.14	1.17	0.52	9.4	80	0.5	100	[18]
MSCI 825 EW	2021	Decal	0.10	0.03	1.90	1.14	1.18	0.53	9.4	80	0.5	100	[18]
HOPI 90% RH (IR corrected)	2021	Decal	0.12	0.20	0.97	0.58	1.20	0.46	3.8	80	0	90	[14]

(continued on next page)

Table 1 (*continued*)

	Year	Fabrication method	Cathode loading (Pt)	Anode loading (Pt)	Current density@0.6V	Power density @0.6V	Peak power density	Peak voltage	Peak Pt utilization	T	Back-pressure	RH	Ref.
Nafion 1100 EW 90% RH (IR-corrected)	2021	Decal	0.12	0.20	0.97	0.58	1.08	0.44	3.4	80	0	90	[14]
HOPI 60% RH (IR corrected)	2021	Decal	0.12	0.20	0.74	0.44	0.93	0.43	2.9	80	0	60	[14]
Nafion 1100 EW 60% RH (IR-corrected)	2021	Decal	0.12	0.20	0.52	0.31	0.87	0.40	2.7	80	0	60	[14]
Carbon support materials													
KB EC300J high humidity	2020	Decal	0.06	0.03	1.67	1.00	0.95	0.55	11.2	80	0.5	100	[72]
KB EC300J low humidity	2020	Decal	0.10	0.03	2.08	1.25	1.23	0.61	9.8	80	1.5	65	[72]
Similar HSC high humidity	2020	Decal	0.06	0.03	1.50	0.90	1.11	0.49	13.1	80	0.5	100	[72]
Similar HSC low humidity	2020	Decal	0.10	0.03	1.45	0.87	1.00	0.50	8.0	80	1.5	65	[72]
Acessible micropourous (HSC-f) 50 cm^2 cell, 65% RH	2018	Decal	0,06	0,025	>2	1,20	1,33	0,66	15,6	94	1,5	65	[75]
Ketjen Black EC300J (HSC-a) 50 cm^2 cell, 65% RH	2018	Decal	0.06	0.025	1.90	1.14	1.16	0.58	13.6	94	1.5	65	[75]
Vulcan XC72, 50 cm^2 cell, 65% RH	2018	Decal	0.06	0.025	1.90	1.14	1.16	0.58	13.6	94	1.5	65	[75]

[a] Platinum loading is 0 mg cm^{-2} since the catalyst has no platinum. In all referenced studies the Fe-N-C catalyst loading was 4 mg cm^{-2}.

Table 2
Performance data from different fabrication methods extracted from polarization curves of various publications discussed in this review. To enhance comparability only results which were recorded in H2/air and which used a Pt/C catalyst are shown. If several different MEAs were investigated in one publication, only the best performing FC is considered.

Fabrication method	Year	Cathode loading (Pt)	Anode loading (Pt)	Current density@0.6V	Pt utilization @0.6V	Power density @0.6V	Peak power density	Peak voltage	Peak Pt utilization	T	Backpressure	RH	Ref.
		[mg cm^{-2}]	[mg cm^{-2}]	[A cm^{-2}]	[W mg_{Pt}^{-1}]	[W cm^{-2}]	[W cm^{-2}]	[V]	[W mg_{Pt}^{-1}]	[°C]	[bar]	[%]	
Slot die Coating - membrane coated onto anode	2012	0.3	0.3	0.85	0.85	0.5	0.61	0.47	1.02	–	–	–	[93]
Electrospinning	2009	0.2	0.2	0.98	1.5	0.59	–	–	–	–	–	–	[114]
Electrospinning	2011	0.1	0.4	0.87	1.0	0.52	0.59	0.50	1.2	80	ambient	100	[117]
Electrospinning	2019	0.1	0.1	1.4	4.2	0.84	0.88	0.52	4.4	80	2	100	[123]
Electrospinning	2021	0.1	0.1	1.54	4.6	0.93	0.98	0.54	4.9	80	1.5	100	[124]
Electrospinning	2021	0.05	0.1	0.80	3.2	0.48	0.69	0.45	4.6	80	1.5	75	[98]
Ultrasonic GDE	2011	0.15	0.05	0.92[a]	2.8[a]	0.55[a]	0.59[a]	0.51[a]	3.0[a]	70	2	50	[97]
Ultrasonic CCM	2017	0.33[b]		1.06	1.9	0.63	0.64	0.54	1.9	80	ambient	100	[86]
Ultrasonic CCM	2021	0.05	0.1	0.61	2.5	0.4	0.53	0.43	3.5	80	1.5	75	[98]
RSDT	2015	0.07	0.07	0.63	2.7	0.38	0.45	0.50	3.2	80	ambient	100	[99]
RSDT	2015	0.1	0.05	0.77	3.1	0.46	0.49	0.54	3.3	80	ambient	100	[102]
Graded CL - RSDT	2017	0.11	0.05	0.67	2.5	0.40	0.43	0.54	2.7	80	ambient	100	[104]
Graded CL - Spraying + EPD	2019	0.3	0.164	1.02	1.33	0.62	0.63	0.57	1.35	80	1.5	100	[141]
Graded CL - Ultrasonic	2022	0.4[c]	0.1	1.5	1.8	0.90	0.96	0.51	1.9	95	2.5	80	[136]

[a] Hydrogen/Oxygen used instead of Hydrogen/Air.
[b] Total loading.
[c] PtCo/C catalyst used.

that the anode is still reliant on platinum to catalyse HOR. *Osmieri* et al. [40] however showed that the anode platinum loading can be lowered up to 0.035 mg cm^{-2} without significantly influencing performance (see also Table 1). Thereby they reached very high Pt-utilisations of 8.8 W mg_{Pt}^{-1} - a very high value within the compared electrode materials, only topped by *Yarlagadda* et al. [75] and *Ramaswamy* et al. [72] in their investigations on carbon supports. Furthermore, they investigated the effect of unnecessarily thickening the cathode catalyst layer by high catalyst loading [40]. 4 mg cm^{-2} was found to be the ideal compromise to achieve high enough activity without increasing mass transport limitations. *Uddin* et al. [41] and showed very similar results to *Osmieri* et al. with high power densities of 0.61 W cm^{-2} at 0.44 V and 0.48 W cm^{-2} at

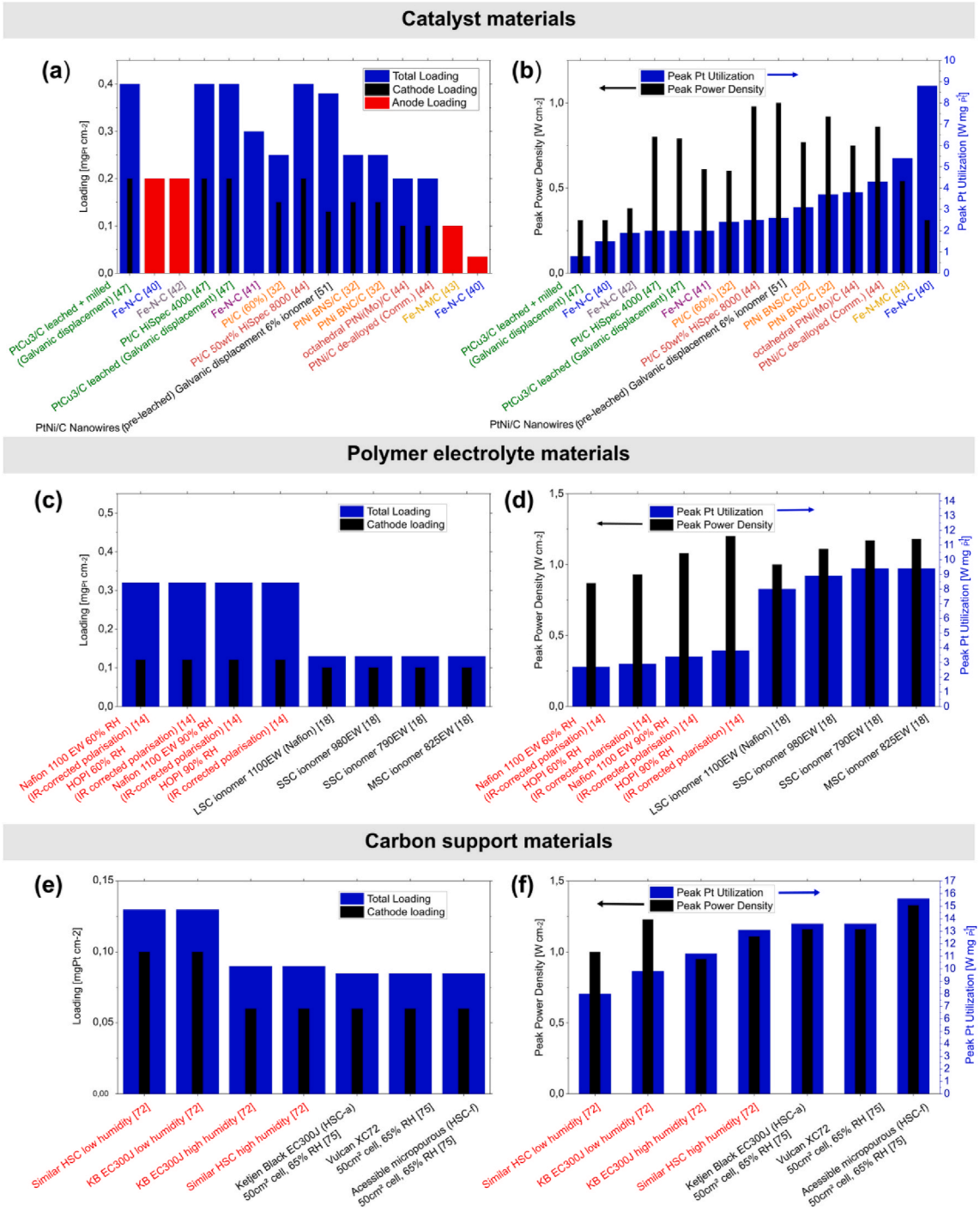

Fig. 6. Platinum loadings (a,c,e) and achieved peak power and platinum utilization (b,d,f) reported in various catalyst, ionomer and carbon support optimization studies. Values were extracted from published polarization curves. Values taken from one reference are given in the same colour. Pt/C type catalysts used as benchmark are reported for better comparability between laboratories. For PGM free catalysts the cathode loading is reported as 0 mg_{Pt} cm^{-2} as only the anode contains Pt. All PGM-free cathodes compared used 4 $mg_{catalyst}$ cm^{-2}. (For interpretation of the references to colour in this figure legend, the reader is referred to the Web version of this article.)

0.6 V. *An* et al. [43] showed how the performance of PGM-free cathodes can be drastically improved by a factor of ~1.6 by preparing Fe-N-MC (MC = mesoporous carbon) from a procedure involving a ferrocene precursor, a Zr-containing MOF called "UiO-66" and graphitic carbon nitride.

At this stage of research on PGM-free catalysts for PEFCs there are still challenges of fast performance decay [41,42] to be overcome and power densities at 0.6 V are still higher for platinum based catalyst systems (see Table 1). However, the reported results show the high potential of Fe-N-C materials to completely replace platinum in PEFC cathodes.

4.1.2. Polymer electrolyte and carbon support materials

A big challenge for low platinum loadings in the catalyst layer during electrode manufacturing is the complete coverage of Pt particles with ionomer. This blocks oxygen access and results in even lower proton

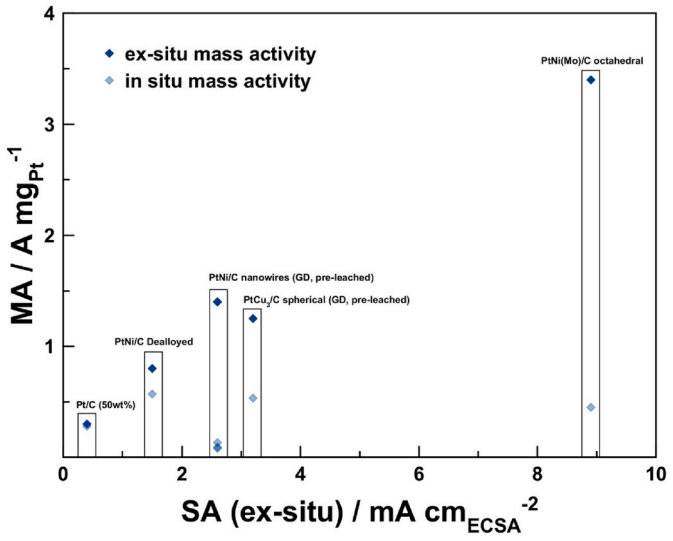

Fig. 7. Mass activities measured in-situ and ex-situ on the same material and by the same group plotted versus the specific activity measured on the RDE. The square bars mark, which is the same material.

conductivity in the vicinity of the platinum surface due to confinement effects [161,162]. During ink preparation, the sulfonic acid functional groups of the ionomer adsorb strongly on the platinum particles increasing the density of the polymer film around them and hindering self-assembly of the polymer to the typical phase segregated structure of Nafion^{TM}. During operation, this dense polymer film creates a strong diffusion barrier for the oxygen molecules, exacerbating the effect the lower the platinum loading gets, consequently resulting in high voltage losses.

The impact of side chain length and equivalent weight of the PFSA ionomer was very recently studied by Ramaswamy et al. [18]. When ionomers with medium and short side chains (MSCI and SSCI) where used, the voltage losses attributed to the catalyst layer where drastically reduced at the limiting current density of 2.5 A cm^{-2}. While the conventional long side chain (LSCI) ionomers Nafion^{TM} D2020 and D2021 exhibit high equivalent weights between 950 and 1100 g/mmol, the MSCI and SSCI exhibit lower EWs of 720–1000 g/mmol. This change in equivalent weight leads to much higher water uptake and the cell voltage at the limiting current density increased sharply by almost +150 mV at EW < 870 g/mmol, where it remained constant. Measurements of the limiting current density at low oxygen partial pressure revealed that the voltage increases were mainly caused by higher proton conductivities in the active layer. Since the equivalent weight of SSCI and MSCI ionomers is much lower, it is possible to manufacture active layers with lower ionomer to carbon ratios, but still obtaining the same proton molality. This way thinner ionomer layers decrease the local oxygen transport resistance, while proton conductivity is almost unaffected. In total this led to a ~20% increase in platinum utilization.

Alternatively, the development of the HOPI revealed that a ~10% higher peak power density can be achieved with the new ionomer type, compared to MEAs using the conventional Nafion^{TM} 1100 EW ionomer [14]. The improvement is most prominent at a lower relative humidification of 70% and in the mass transport limited region of the polarization curve, confirming that the improved gas transport of the new ionomer leads to this performance increase. In Fig. 6(c–d), it seems that LSCI and MSCI ionomers clearly outperform the HOPI type in terms of platinum utilization. It must be pointed out, however, that there is a considerable difference in the anode loading, backpressure and measurement temperature (Table 1). It is not unusual that very high anode loadings are used in cathode development studies to avoid anode activation losses. However, the results of studies with very high platinum utilization in Table 1 and Fig. 6 all suggest that anode loadings between 0.025 and 0.1 mg cm^{-2} are viable without significant performance losses.

Similar to the developments with higher oxygen permeability ionomers, the carbon support microstructure plays a crucial role in oxygen transport [72–75]. General Motors studied the influence of high surface area carbons (HSC) on kinetics and local oxygen and proton transport limitations and compared it to medium surface area carbons (MSC) like Vulcan XC72 (Fig. 6(e–f), Table 1). Oxygen must pass through the microporous (<2 nm) openings on the carbon particle surface to reach the Pt-alloy nanoparticles present within the mesoporous regions, which poses a major resistance and leads to significant cell voltage losses at high current densities. At the same time, the ionomer distribution and therefore bulk proton conductivity was found to be directly correlated to the mesoporous (>2 nm) volume. Thereby, a shift in microporous volume towards meso- and macroporous volume benefits the oxygen transport near the catalyst particle surface, whereas the opposite shift strongly benefits bulk proton transport in the ionomer phase of the catalyst layer and platinum distribution. The difference between Ketjen Black and Vulcan carbons in this respect can be summed up in the former being beneficial for kinetic performance due to its high surface area, which results in highly distributed platinum. The high surface area is achieved through large microporous volume fractions, which leads to partly inaccessible particles and hence insufficient mass transport. Vulcan on the other hand shows lower surface area, leading to worse kinetic performance and better mass transport. Following this approach, General Motors developed a type of carbon deemed "accessible microporous carbon" and labelled "HSC-f" with a surface area of 698 m^2 g^{-1}, which clearly outperformed Ketjen Black and Vulcan and even showed positive effects on lifetime [72–75]. This was achieved by maximizing the mesoporous volume and minimizing the macroporous volume using a non-disclosed procedure.

4.2. Effects of the manufacturing method

4.2.1. Influence of the coating technique

The platinum loading of electrodes produced with various manufacturing methods is displayed in Fig. 8a. Fig. 8b displays the peak Pt utilization and peak power density of fuel cells using electrodes produced with the respective methods. It is evident from Fig. 8(a–b) that RSDT, electrospinning and ultrasonic spray coating can all achieve total loadings at or even below 0.2 mg_{Pt} cm^{-2}, while maintaining high peak power densities. Note that the catalyst loading, and peak Pt utilization change significantly depending on the method, yet there is no obvious trend for the peak power density, which is within 0.71 ± 0.28 W cm^{-2} for all methods.

Of all the discussed electrode manufacturing methods, slot die coating [93] is the process with the lowest reported peak platinum utilization. High anode loadings might have resulted in the low platinum utilization. However, the cathode loading in the study was also considerably higher than in those references where other manufacturing methods had been used. The low performance of this method could also be explained by mass transport limitations through the non-porous, thin film catalyst layer. Furthermore, the viscous catalyst slurry employed in this method might promote agglomeration of platinum particles, blocking catalytically active sites. A significant performance increase can be achieved with ultrasonic spray coating [98]. The ultrasonic spraying nozzle forms micron sized droplets, which force platinum agglomerates to separate from each other, and hence a better performance is accomplished. A similarly high peak platinum utilization with values above 3 W mg_{Pt}^{-1} are achieved by the RSDT process [102]. This is reasonable, because in contrast to the use of heterogeneous catalyst slurries, direct deposition of freshly synthesized platinum particles onto the membrane has never been observed to cause agglomeration. Furthermore, premixing of catalyst support and ionomer can be utilized to increase the ionomer coverage. Finally, the platinum utilization of

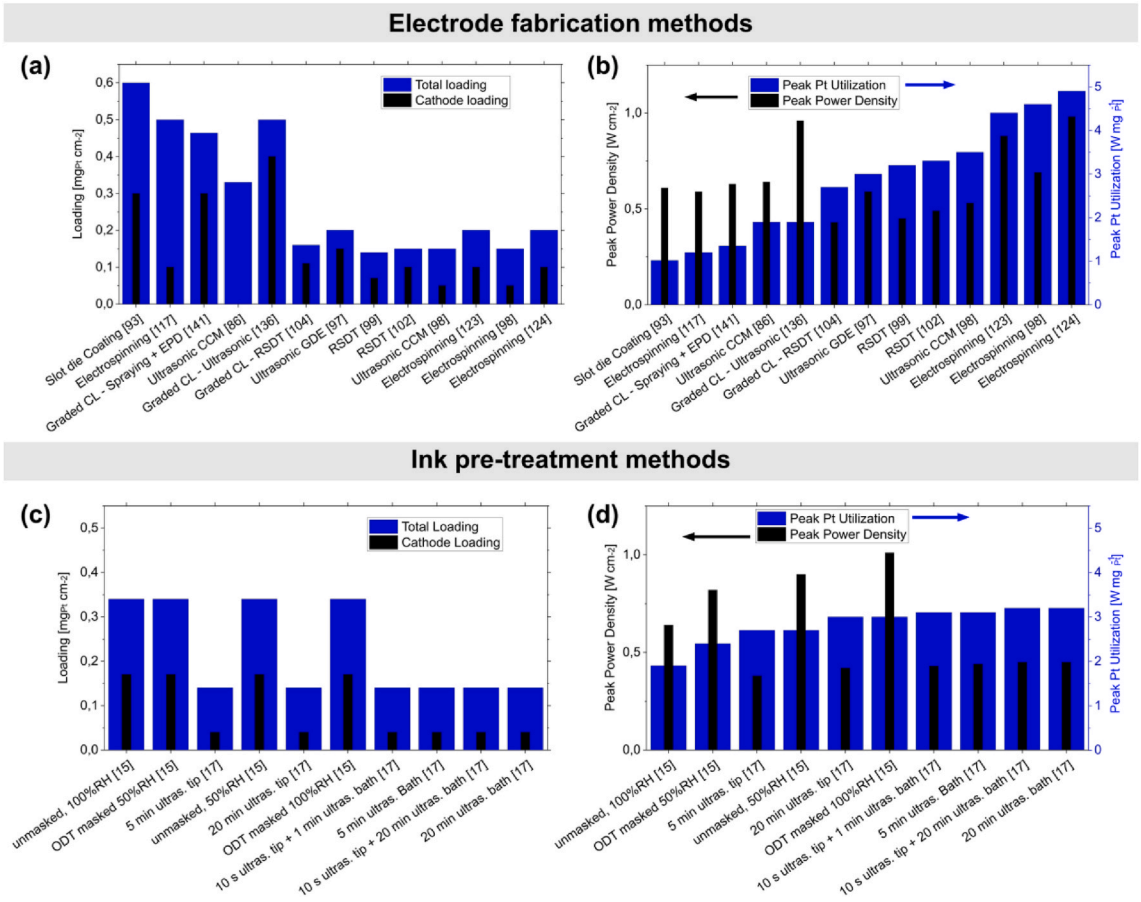

Fig. 8. Cathode as well as total catalyst loading (a,c) and peak power density and peak Pt utilization (b,d) of different electrode and MEA manufacturing and ink pre-treatment methods. The number in square brackets refers to the referenced publication. Performance data was extracted from polarization curves in the references and is summarized in Table 2 for the electrode fabrication methods and Table 1 for the ink pre-treatment methods.

electrospun electrodes consistently show the highest Pt utilization with values above 4 W mg_{Pt}^{-1} and only one exception [117], where a high anode loading of 0.4 mg_{Pt} cm^{-2} was used. This large performance gain is explained by two main factors: i) de-agglomeration of the platinum particles due to the extreme shear forces in the catalyst ink jet during deposition and ii) excellent mass transport due to the large inter-fibre voids.

Considering the topic of graded catalyst layers, it is not straight forward to compare them in a standardized manner since the introduced literature focuses on either optimizing the catalyst particle size [104], the ionomer content [136] or they combine different manufacturing methods [141]. However, a performance increase relative to internal standards was noted in each of the studies.

4.2.2. *Effects of ink and material pre-treatment*

The effect of ink pre-treatment methods on power density and platinum utilization is shown in Fig. 8(c–d). Most active layer manufacturing methods rely on inks or slurries composed of the carbon supported catalyst, the ion conducting polymer (ionomer) and a solvent or solvent mixture. The exact composition, the used mixing tools and the methodology of mixing have a significant impact on the final performance and must therefore be extensively studied and refined. They have a strong influence on the distribution of the ionomer and how well carbon agglomerates (diameter, d = 1–10 μm) and aggregates (d = 100–300 nm) are broken up. The effects of ultrasonic wave power and exposure time on the ECSA and power output of the produced catalyst layer was systematically studied by *Pollet* et al. [76] and *Wang* et al. [17]. While high power sonication with tip probes (3–12 W) proved effective in breaking up carbon agglomerates and aggregates quickly, prolonged sonication led to detachment of platinum particles from the support and even agglomeration. This has a negative effect on the ECSA and power output of the resulting catalyst layer. Prolonged (20–30 min) low power (~2 W) bath sonication resulted in a sufficient break-up of agglomerates without damaging the platinum particles, thereby increasing the ECSA. A combination of short probe sonication and prolonged low power bath sonication effectively broke up agglomerates and aggregates without detachment of platinum. Proper ink processing increased the ECSA on the RDE, which had already been shown by *Pollet* et al. [76]. This trend could be reproduced in the MEA by Wang et al. [17]. Improvements in power density and in-situ ECSA in the single cell were achieved by proper ultrasonic mixing.

All the previously mentioned developments produced ionomer films on particles that inherently create an oxygen barrier. While there is a certain range in which the film thickness can be varied by the ionomer structure, very few methods have yet been reported that exactly control, where the ionomer is deposited. Octadecanethiol (ODT) has been used by *Doo* et al. [15] as masking agent for the platinum particles to avoid thick films of ionomer around the Pt-surface. This effectively improved mass transport without significantly hindering proton conduction by the absence of a direct ionomer/platinum interface. The masking agent could be electrochemically removed by cycling in fully humidified hydrogen at the anode and nitrogen at the cathode to oxidize and wash out the soluble ODT oxidation products without having a noticeable effect on MEA performance [15]. This chemical pre-treatment of the catalyst effectively increased the power density of the produced MEA at a low relative humidity of 50%. The distance between ionomer-rich areas and the ionomer-lean platinum particles seems to be short

enough to allow proper proton transport via an alternative mechanism. Such an "electrolyteless" proton transport had already been observed by *Kim* et al. over distances of ~1 μm [163]. Assuming that ODT lengths are in the range of 1.8–3 nm, as observed on Au, Ag and Pt surfaces [164, 165], it is safe to conclude that the ionomer does not need to be in direct contact with the platinum particles. A drawback of this method are the residues of the masking agent, which could have long-term effects on the MEA performance. They have to be studied before this intriguing concept can be further developed into a commercially available fuel cell MEA.

5. Conclusions

The latest advances in the field of materials development and manufacturing methods for PEFCs were reviewed in detail and major trends were found and analysed component by component. Fortunately, references with data from industrial R&D departments were available and could also be included. By combining the knowledge found in literature, the following promising pathways were identified to increase performance, platinum utilization and lifetime in the future:

- Increasing the ECSA of catalysts by unusually high specific activity, developing methods to mitigate poisoning by the sulfonic acid groups in the PFSA or increasing the oxygen accessibility, e.g., by using highly mesoporous carbon supports.
- Determination of the effect of the bond strength of the sulfonic acid groups on the crystal planes such as PtNi(111) the in-situ activity.
- Improvement of local oxygen transport to the active sites by PFSA modification (e.g. HOPI-approach) or chemical masking (e.g. ODT-approach).
- Increase proton conductivity by using ionomers with short side chain to thereby maintain proton conductivity at lower ionomer content and indirectly increase oxygen permeability.
- Improve and optimize ink-mixing techniques and determine their impact on the newly developed materials.
- Investigate the lifetime and degradation mechanisms of non-precious metal components over extended operating periods.
- Upscaling and industrialization of coating methods such as ultrasonic spray coating or electrospinning to production rates achieved in slot die coating.

Finally, harmonization of test procedures, reporting practices (e.g. material nomenclature) and hardware has considerably improved over the past decade. Further specialization in standardized test procedures for individual material classes, individual components, up to test procedures of the entire fuel cell, including both hardware and test protocols, would be of great benefit for future rapid progress.

CRediT authorship contribution statement

M. Grandi: Conceptualization, Methodology, Writing – original draft, Writing – review & editing, Data curation, Visualization. **S. Rohde:** Conceptualization, Methodology, Writing – original draft, Writing – review & editing, Data curation, Visualization. **D.J. Liu:** Writing – review & editing. **B. Gollas:** Conceptualization, Writing – review & editing, Supervision. **V. Hacker:** Conceptualization, Writing – review & editing, Supervision, Project administration, Funding acquisition.

Declaration of competing interest

The authors declare that they have no known competing financial interests or personal relationships that could have appeared to influence the work reported in this paper.

Data availability

No data was used for the research described in the article.

Acknowledgements

Financial support was provided by the IEA Research Cooperation (Technology Collaboration Programme on Advanced Fuel Cells AFC TCP of the International Energy Agency). The project is being carried out as part of the IEA research cooperation on behalf of the Federal Ministry for Climate Action and Energy (bmk). Further Financial support was provided by the "Zukunftsfonds Steiermark" of the "Amt der Steiermärkischen Landesregierung" (Office of the Styrian Provincial Government), under the grant number PN 1312. We acknowledge financial support by a European Space Agency (ESA) Open Science Innovation Platform study (contract no. 4000135234/21/NL/GLC/my).

Abbreviations

AB	Acetylene black
CCM	Catalyst coated membrane
CL	Catalyst layer
DMD	Direct Membrane Deposition
DOE	Department of energy
ECSA	Electrochemical surface area
EPD	Electrophoresis deposition
EW	Equivalent weight
GDE	Gas diffusion electrode
GDL	Gas diffusion layer
HOPI	High oxygen permeability ionomer
HOR	Hydrogen oxidation reaction
HSC	High surface carbon
IEC	Ion Exchange capacity
KB	Ketjen black EC300J
LSCI	Long side chain ionomer
MA	Mass activity
MEA	Membrane electrode assembly
MSCI	Medium side chain ionomer
MSC	medium surface carbon
ODT	Octadecane thiol
ORR	Oxygen reduction reaction
PAA	Poly acrylic acid
PEFC	Polymer electrolyte fuel cell
PEO	Poly ethylene oxide
PFSA	Perfluorosulfonic acid
RDE	Rotating disc Electrode
RHE	Reversible hydrogen electrode
RSDT	Reactive spray deposition technique
SA	Specific activity
SSCI	Short side chain ionomer
TPB	Triple Phase Boundary
VUL	Vulcan XC72

References

[1] Y. Wang, K.S. Chen, J. Mishler, S.C. Cho, X.C. Adroher, A review of polymer electrolyte membrane fuel cells: technology, applications, and needs on fundamental research, Appl. Energy 88 (2011) 981–1007, https://doi.org/10.1016/j.apenergy.2010.09.030.
[2] O.Z. Sharaf, M.F. Orhan, An overview of fuel cell technology: fundamentals and applications, Renew. Sustain. Energy Rev. 32 (2014) 810–853, https://doi.org/10.1016/J.RSER.2014.01.012.
[3] A. Wilson, G. Kleen, D. Papageorgopoulos, DOE Hydrogen and Fuel Cells Program Record, 2017.
[4] E.J. Carlson, P. Kopf, J. Sinha, S. Sriramulu, Y. Yang, Cost analysis of PEM fuel cell systems for transportation: september 30, 2005, Golden, CO, CO, https://doi.org/10.2172/862302, 2005.
[5] H.U. Sverdrup, K.V. Ragnarsdottir, A system dynamics model for platinum group metal supply, market price, depletion of extractable amounts, ore grade,

recycling and stocks-in-use, Resour. Conserv. Recycl. 114 (2016) 130–152, https://doi.org/10.1016/j.resconrec.2016.07.011.
[6] E.J. Carlson, P. Kopf, J. Sinha, S. Sriramulu, Y. Yang, Cost analysis of PEM fuel cell systems for transportation: september 30, 2005, Golden, CO, https://doi.org/10.2172/862302, 2005.
[7] H.U. Sverdrup, K.V. Ragnarsdottir, A system dynamics model for platinum group metal supply, market price, depletion of extractable amounts, ore grade, recycling and stocks-in-use, Resour. Conserv. Recycl. 114 (2016) 130–152, https://doi.org/10.1016/j.resconrec.2016.07.011.
[8] V. Mehta, J.S. Cooper, Review and analysis of PEM fuel cell design and manufacturing, J. Power Sources 114 (2003) 32–53, https://doi.org/10.1016/S0378-7753(02)00542-6.
[9] C.Y. Liu, C.C. Sung, A review of the performance and analysis of proton exchange membrane fuel cell membrane electrode assemblies, J. Power Sources 220 (2012) 348–353, https://doi.org/10.1016/j.jpowsour.2012.07.090.
[10] A. De las Heras, F.J. Vivas, F. Segura, J.M. Andújar, From the cell to the stack. A chronological walk through the techniques to manufacture the PEFCs core, Renew. Sustain. Energy Rev. 96 (2018) 29–45, https://doi.org/10.1016/j.rser.2018.07.036.
[11] J. Ouimet R, A. Ebaugh T, G. Mirshekari, S. Bliznakov, J. Bonville L, R. Maric, Current status on the manufacturing of nanomaterials for proton exchange membrane energy systems by vapor-based processes, Energy Fuel. 35 (2021) 1933–1956, https://doi.org/10.1021/acs.energyfuels.0c03670.
[12] S. Litster, G. McLean, PEM fuel cell electrodes, J. Power Sources 130 (2004) 61–76, https://doi.org/10.1016/j.jpowsour.2003.12.055.
[13] R. O'Hayre, D.M. Barnett, F.B. Prinz, The triple phase boundary: a mathematical model and experimental investigations for fuel cells, J. Electrochem. Soc. 152 (2005) A439, https://doi.org/10.1149/1.1851054.
[14] R. Jinnouchi, K. Kudo, K. Kodama, N. Kitano, T. Suzuki, S. Minami, et al., The role of oxygen-permeable ionomer for polymer electrolyte fuel cells, Nat. Commun. 12 (2021), https://doi.org/10.1038/s41467-021-25301-3.
[15] G. Doo, S. Yuk, J.H. Lee, S. Choi, D.H. Lee, D.W. Lee, et al., Nano-scale control of the ionomer distribution by molecular masking of the Pt surface in PEMFCs, J. Mater. Chem. 8 (2020) 13004–13013, https://doi.org/10.1039/c9ta14002f.
[16] N. Ramaswamy, W. Gu, J.M. Ziegelbauer, S. Kumaraguru, Carbon support microstructure impact on high current density transport resistances in PEMFC cathode, J. Electrochem. Soc. 167 (2020), 064515, https://doi.org/10.1149/1945-7111/ab819c.
[17] M. Wang, J.H. Park, S. Kabir, K.C. Neyerlin, N.N. Kariuki, H. Lv, et al., Impact of catalyst ink dispersing methodology on fuel cell performance using in-situ X-ray scattering, ACS Appl. Energy Mater. 2 (2019) 6417–6427, https://doi.org/10.1021/acsaem.9b01037.
[18] N. Ramaswamy, S. Kumaraguru, R. Koestner, T. Fuller, W. Gu, N. Kariuki, et al., Editors' choice—ionomer side chain length and equivalent weight impact on high current density transport resistances in PEMFC cathodes, J. Electrochem. Soc. 168 (2021), 024518, https://doi.org/10.1149/1945-7111/abe5eb.
[19] J. Liu, E. Medici, A.T. Haug, D.A. Cullen, K. Tajiri, J.S. Allen, et al., Coupled continuum and network model framework to study catalyst layers of polymer electrolyte fuel cells, Int. J. Hydrogen Energy 47 (2022) 17749–17761, https://doi.org/10.1016/j.ijhydene.2022.03.266.
[20] DOE Technical Targets for Polymer Electrolyte Membrane Fuel Cell Components (n.d).
[21] P. Jovanovič, V.S. Šelih, M. Šala, S.B. Hočevar, A. Pavlišič, M. Gatalo, et al., Electrochemical in-situ dissolution study of structurally ordered, disordered and gold doped PtCu3 nanoparticles on carbon composites, J. Power Sources 327 (2016) 675–680, https://doi.org/10.1016/j.jpowsour.2016.07.112.
[22] M. Gatalo, L. Moriau, U. Petek, F. Ruiz-Zepeda, M. Šala, M. Grom, et al., CO-assisted ex-situ chemical activation of Pt-Cu/C oxygen reduction reaction electrocatalyst, Electrochim. Acta 306 (2019) 377–386, https://doi.org/10.1016/j.electacta.2019.03.153.
[23] M. Gatalo, N. Hodnik, M. Bele, P. Jovanovič, M. Gaberšček, M. Grom, Method of Treating a Platinum-Alloy Catalyst, and Device for Carrying Out the Method of Treating a Platinum-Alloy Catalyst, 2018. EP18196870.2.
[24] M. Gatalo, F. Ruiz-Zepeda, N. Hodnik, G. Dražić, M. Bele, M. Gaberšček, Insights into thermal annealing of highly-active PtCu3/C Oxygen Reduction Reaction electrocatalyst: an in-situ heating transmission Electron microscopy study, Nano Energy 63 (2019), 103892, https://doi.org/10.1016/j.nanoen.2019.103892.
[25] M. Gatalo, P. Jovanovič, U. Petek, M. Šala, V.S. Šelih, F. Ruiz-Zepeda, et al., Comparison of Pt–Cu/C with benchmark Pt–Co/C: metal dissolution and their surface interactions, ACS Appl. Energy Mater. (2019), https://doi.org/10.1021/acsaem.8b02142.
[26] M. Bele, P. Jovanovič, A. Pavlišič, B. Jozinović, M. Zorko, A. Rečnik, et al., A highly active PtCu3 intermetallic core-shell, multilayered Pt-skin, carbon embedded electrocatalyst produced by a scale-up sol-gel synthesis, Chem. Commun. 50 (2014) 13124–13126, https://doi.org/10.1039/c4cc05637j.
[27] M. Gatalo, M. Bele, F. Ruiz Zepeda, E. Šest, M. Šala, A.R. Kamšek, et al., A double-passivation water-based galvanic displacement method for reproducible gram-scale production of high-performance platinum-alloy electrocatalysts, Angew. Chem. Int. Ed. 58 (2019) 13266–13270, https://doi.org/10.1002/anie.201903568.
[28] S.M. Alia, B.A. Larsen, S. Pylypenko, D.A. Cullen, D.R. Diercks, K.C. Neyerlin, et al., Platinum-coated nickel nanowires as oxygen-reducing electrocatalysts, ACS Catal. 4 (2014) 1114–1119, https://doi.org/10.1021/cs401081w.
[29] Y. Holade, K. Servat, T.W. Napporn, K.B. Kokoh, Electrocatalytic properties of nanomaterials synthesized from "Bromide Anion Exchange" method - investigations of glucose and glycerol oxidation, Electrochim. Acta 162 (2015) 205–214, https://doi.org/10.1016/j.electacta.2014.11.072.
[30] P. Tonda-Mikiela, T.W. Napporn, C. Morais, K. Servat, a. Chen, K.B. Kokoh, Synthesis of gold-platinum nanomaterials using bromide anion exchange-synergistic electroactivity toward CO and glucose oxidation, J. Electrochem. Soc. 159 (2012) H828–H833, https://doi.org/10.1149/2.001211jes.
[31] S.-I. Choi, S. Xie, M. Shao, J.H. Odell, N. Lu, H.-C. Peng, et al., Synthesis and characterization of 9 nm Pt–Ni octahedra with a record high activity of 3.3 A/mg Pt for the oxygen reduction reaction, Nano Lett. 13 (2013) 3420–3425, https://doi.org/10.1021/nl401881z.
[32] X. Tian, X. Zhao, Y.-Q. Su, L. Wang, H. Wang, D. Dang, et al., Engineering bunched Pt-Ni alloy nanocages for efficient oxygen reduction in practical fuel cells, Science 366 (2019) 850–856, https://doi.org/10.1126/science.aaw7493.
[33] C. Cui, L. Gan, H.-H. Li, S.-H. Yu, M. Heggen, P. Strasser, Octahedral PtNi nanoparticle catalysts: exceptional oxygen reduction activity by tuning the alloy particle surface composition, Nano Lett. 12 (2012) 5885–5889, https://doi.org/10.1021/nl3032795.
[34] X. Huang, Z. Zhao, L. Cao, Y. Chen, E. Zhu, Z. Lin, et al., High-performance transition metal–doped Pt 3 Ni octahedra for oxygen reduction reaction, Science 348 (2015) 1230–1234, https://doi.org/10.1126/science.aaa8765.
[35] S. Kühl, H. Heyen, P. Strasser, Mo-doped Shaped Nanoparticles Based on PtNi-Alloys – A Promising ORR Catalyst?, 75, 2016, pp. 723–730.
[36] C. Cui, L. Gan, M. Heggen, S. Rudi, P. Strasser, Compositional segregation in shaped Pt alloy nanoparticles and their structural behaviour during electrocatalysis, Nat. Mater. 12 (2013) 765–771, https://doi.org/10.1038/nmat3668.
[37] B.-A. Lu, T. Sheng, N. Tian, Z.-C. Zhang, C. Xiao, Z.-M. Cao, et al., Octahedral PtCu alloy nanocrystals with high performance for oxygen reduction reaction and their enhanced stability by trace Au, Nano Energy 33 (2017) 65–71, https://doi.org/10.1016/j.nanoen.2017.01.003.
[38] X. Zhao, S. Chen, Z. Fang, J. Ding, W. Sang, Y. Wang, et al., Octahedral Pd@Pt 1.8 Ni core–shell nanocrystals with ultrathin PtNi alloy shells as active catalysts for oxygen reduction reaction, J. Am. Chem. Soc. 137 (2015) 2804–2807, https://doi.org/10.1021/ja511596c.
[39] H. Wang, B. Chen, D. Liu, Metal–organic frameworks and metal–organic gels for oxygen electrocatalysis: structural and compositional considerations, Adv. Mater. 33 (2021), 2008023, https://doi.org/10.1002/adma.202008023.
[40] L. Osmieri, H. Wang, K.C. Neyerlin, Impact of fabrication and testing parameters on the performance of a polymer electrolyte fuel cell with platinum group metal (PGM)-Free cathode catalyst, J. Electrochem. Soc. 168 (2021), 014503, https://doi.org/10.1149/1945-7111/abd48e.
[41] A. Uddin, L. Dunsmore, H. Zhang, L. Hu, G. Wu, S. Litster, High power density platinum group metal-free cathodes for polymer electrolyte fuel cells, ACS Appl. Mater. Interfaces 12 (2020) 2216–2224, https://doi.org/10.1021/acsami.9b13945.
[42] L. Osmieri, D.A. Cullen, H.T. Chung, R.K. Ahluwalia, K.C. Neyerlin, Durability evaluation of a Fe–N–C catalyst in polymer electrolyte fuel cell environment via accelerated stress tests, Nano Energy 78 (2020), 105209, https://doi.org/10.1016/j.nanoen.2020.105209.
[43] L. An, B. Chi, Y. Deng, C. Chen, X. Deng, R. Zeng, et al., Engineering g-C3N4 composited Fe-UIO-66 to in-situ generate robust single-atom Fe sites for high-performance PEMFC and Zn-air battery, J. Mater. Chem. (2022), https://doi.org/10.1039/D2TA07962C.
[44] F. Dionigi, C.C. Weber, M. Primbs, M. Gocyla, A.M. Bonastre, C. Spöri, et al., Controlling near-surface Ni composition in octahedral PtNi(Mo) nanoparticles by Mo doping for a highly active oxygen reduction reaction catalyst, Nano Lett. 19 (2019) 6876–6885, https://doi.org/10.1021/acs.nanolett.9b02116.
[45] X. Zhao, S. Chen, Z. Fang, J. Ding, W. Sang, Y. Wang, et al., Octahedral Pd@Pt1.8Ni core-shell nanocrystals with ultrathin PtNi alloy shells as active catalysts for oxygen reduction reaction, J. Am. Chem. Soc. 137 (2015) 2804–2807, https://doi.org/10.1021/ja511596c.
[46] P. Mani, R. Srivastava, P. Strasser, Dealloyed binary PtM 3(M = Cu, Co, Ni) and ternary PtNi3M (M = Cu, Co, Fe, Cr) electrocatalysts for the oxygen reduction reaction: performance in polymer electrolyte membrane fuel cells, J. Power Sources 196 (2011) 666–673, https://doi.org/10.1016/j.jpowsour.2010.07.047.
[47] M. Bele, M. Gatalo, P. Jovanovič, F. Ruiz-Zepeda, M. Šala, E. Šest, et al., Insight on single cell proton exchange membrane fuel cell performance of Pt-Cu/C cathode, Catalysts 9 (2019) 544.
[48] P. Strasser, Dealloyed core-shell fuel cell electrocatalysts, Rev. Chem. Eng. 25 (2009) 255.
[49] M. Gatalo, L. Moriau, U. Petek, F. Ruiz-Zepeda, M. Šala, M. Grom, et al., CO-assisted ex-situ chemical activation of Pt-Cu/C oxygen reduction reaction electrocatalyst, Electrochim. Acta 306 (2019) 377–386, https://doi.org/10.1016/j.electacta.2019.03.153.
[50] B.A. Lu, T. Sheng, N. Tian, Z.C. Zhang, C. Xiao, Z.M. Cao, et al., Octahedral PtCu alloy nanocrystals with high performance for oxygen reduction reaction and their enhanced stability by trace Au, Nano Energy 33 (2017) 65–71, https://doi.org/10.1016/j.nanoen.2017.01.003.
[51] S.A. Mauger, K.C. Neyerlin, S.M. Alia, C. Ngo, S.K. Babu, K.E. Hurst, et al., Fuel cell performance implications of membrane electrode assembly fabrication with platinum-nickel nanowire catalysts, J. Electrochem. Soc. 165 (2018) F238–F245, https://doi.org/10.1149/2.1061803jes.
[52] K. Jiang, D. Zhao, S. Guo, X. Zhang, X. Zhu, J. Guo, Efficient oxygen reduction catalysis by subnanometer Pt alloy nanowires Efficient oxygen reduction catalysis by subnanometer Pt alloy nanowires, 2–9, https://doi.org/10.1126/sciadv.1601705, 2017.

[53] L. Bu, N. Zhang, S. Guo, X. Zhang, J. Li, J. Yao, et al., Biaxially strained PtPb/Pt core/shell nanoplate boosts oxygen reduction catalysis, Science 354 (2016) 1410–1414, https://doi.org/10.1126/science.aah6133.

[54] Strasser P. Dealloyed Pt Core-Shell Nanoparticles : Active and Durable Electrocatalysts for Low-Temperature Polymer Electrolyte Membrane Fuel Cells (PEMFCs) Strem Chemicals Chemist Finds New Way to Drive to Work (n.d).

[55] T. Yoshida, K. Kojima, Toyota MIRAI fuel cell vehicle and progress toward a future hydrogen society, Interface Magazine 24 (2015) 45–49, https://doi.org/10.1149/2.F03152if.

[56] Y. Xiong, L. Xiao, Y. Yang, F.J. DiSalvo, H.D. Abruña, High-loading intermetallic Pt_3Co/C core-shell nanoparticles as enhanced activity electrocatalyst towards the oxygen reduction reaction (ORR), Chem. Mater. (2018), https://doi.org/10.1021/acs.chemmater.7b04201 acs.chemmater.7b04201.

[57] C. Cui, L. Gan, H.H. Li, S.H. Yu, M. Heggen, P. Strasser, Octahedral PtNi nanoparticle catalysts: exceptional oxygen reduction activity by tuning the alloy particle surface composition, Nano Lett. 12 (2012) 5885–5889, https://doi.org/10.1021/nl3032795.

[58] C. Chen, Y. Kang, Z. Huo, Z. Zhu, W. Huang, H.L. Xin, et al., Highly crystalline multimetallic nanoframes with three-dimensional electrocatalytic surfaces, Science 343 (2014) 1339–1343, https://doi.org/10.1126/science.1249061.

[59] X. Huang, Z. Zhao, L. Cao, Y. Chen, E. Zhu, Z. Lin, et al., High-performance transition metal – doped Pt3Ni octahedra for oxygen reduction reaction, Science 348 (2015) 1230–1234, https://doi.org/10.1126/science.aaa8765.

[60] M. Gatalo, P. Jovanovič, G. Polymeros, J.P. Grote, A. Pavlišič, F. Ruiz- Zepeda, et al., Positive effect of surface doping with Au on the stability of Pt-based electrocatalysts, ACS Catal. 6 (2016) 1630–1634, https://doi.org/10.1021/acscatal.5b02883.

[61] J. Greeley, Structural effects on trends in the deposition and dissolution of metal-supported metal adstructures, Electrochim. Acta 55 (2010) 5545–5550, https://doi.org/10.1016/j.electacta.2010.04.055.

[62] S.A. Mauger, K.C. Neyerlin, S.M. Alia, C. Ngo, S.K. Babu, K.E. Hurst, et al., Fuel cell performance implications of membrane electrode assembly fabrication with platinum-nickel nanowire catalysts, J. Electrochem. Soc. 165 (2018) F238–F245, https://doi.org/10.1149/2.1061803jes.

[63] F. Ruiz-Zepeda, M. Gatalo, A. Pavlišič, G. Dražić, P. Jovanovič, M. Bele, et al., Atomically resolved anisotropic electrochemical shaping of nano-electrocatalyst, Nano Lett. (2019), https://doi.org/10.1021/acs.nanolett.9b00918.

[64] R.K. Ahluwalia, X. Wang, J.K. Peng, N.N. Kariuki, D.J. Myers, S. Rasouli, et al., Durability of de-alloyed platinum-nickel cathode catalyst in low platinum loading membrane-electrode assemblies subjected to accelerated stress tests, J. Electrochem. Soc. 165 (2018) 3316–3327, https://doi.org/10.1149/2.0341806jes.

[65] P. Frühwirt, A. Kregar, J.T. Törring, T. Katrašnik, G. Gescheidt, Holistic approach to chemical degradation of Nafion membranes in fuel cells: modelling and predictions, Phys. Chem. Chem. Phys. 22 (2020) 5647–5666, https://doi.org/10.1039/C9CP04986J.

[66] M. Robert, A. El Kaddouri, J.-C. Perrin, K. Mozet, M. Daoudi, J. Dillet, et al., Effects of conjoint mechanical and chemical stress on perfluorosulfonic-acid membranes for fuel cells, J. Power Sources 476 (2020), 228662, https://doi.org/10.1016/j.jpowsour.2020.228662.

[67] H. Xie, X. Xie, G. Hu, V. Prabhakaran, S. Saha, L. Gonzalez-Lopez, et al., Ta–TiOx nanoparticles as radical scavengers to improve the durability of Fe–N–C oxygen reduction catalysts, Nat. Energy 7 (2022) 281–289, https://doi.org/10.1038/s41560-022-00988-w.

[68] A.M. Baker, R. Mukundan, D. Spernjak, E.J. Judge, S.G. Advani, A.K. Prasad, et al., Cerium migration during PEM fuel cell accelerated stress testing, J. Electrochem. Soc. 163 (2016) F1023–F1031, https://doi.org/10.1149/2.0181609jes.

[69] D.C. Seo, I. Jeon, E.S. Jeong, J.Y. Jho, Mechanical properties and chemical durability of nafion/sulfonated graphene oxide/cerium oxide composite membranes for fuel-cell applications, Polymers 12 (2020) 1375, https://doi.org/10.3390/polym12061375.

[70] R.K. Ahluwalia, S. Arisetty, J.-K. Peng, R. Subbaraman, X. Wang, N. Kariuki, et al., Dynamics of particle growth and electrochemical surface area loss due to platinum dissolution, J. Electrochem. Soc. 161 (2014) F291–304, https://doi.org/10.1149/2.051403jes.

[71] S.M.S. Kumar, N. Hidyatai, J.S. Herrero, S. Irusta, K. Scott, Efficient tuning of the Pt nano-particle mono-dispersion on Vulcan XC-72R by selective pre-treatment and electrochemical evaluation of hydrogen oxidation and oxygen reduction reactions, Int. J. Hydrogen Energy 36 (2011) 5453–5465, https://doi.org/10.1016/j.ijhydene.2011.01.124.

[72] N. Ramaswamy, W. Gu, J.M. Ziegelbauer, S. Kumaraguru, Carbon support microstructure impact on high current density transport resistances in PEMFC cathode, J. Electrochem. Soc. 167 (2020), 064515, https://doi.org/10.1149/1945-7111/ab819c.

[73] E. Padgett, V. Yarlagadda, M.E. Holtz, M. Ko, B.D.A. Levin, R.S. Kukreja, et al., Mitigation of PEM fuel cell catalyst degradation with porous carbon supports, J. Electrochem. Soc. 166 (2019) F198–207, https://doi.org/10.1149/2.0371904jes.

[74] E. Padgett, N. Andrejevic, Z. Liu, A. Kongkanand, W. Gu, K. Moriyama, et al., Editors' choice—connecting fuel cell catalyst nanostructure and accessibility using quantitative cryo-STEM tomography, J. Electrochem. Soc. 165 (2018) F173–F180, https://doi.org/10.1149/2.0541803jes.

[75] V. Yarlagadda, M.K. Carpenter, T.E. Moylan, R.S. Kukreja, R. Koestner, W. Gu, et al., Boosting fuel cell performance with accessible carbon mesopores, ACS Energy Lett. 3 (2018) 618–621, https://doi.org/10.1021/acsenergylett.8b00186.

[76] B.G. Pollet, J.T.E. Goh, The importance of ultrasonic parameters in the preparation of fuel cell catalyst inks, Electrochim. Acta 128 (2014) 292–303, https://doi.org/10.1016/j.electacta.2013.09.160.

[77] L. Chong, J. Wen, J. Kubal, F.G. Sen, J. Zou, J. Greeley, et al., Ultralow-loading platinum-cobalt fuel cell catalysts derived from imidazolate frameworks, Science 362 (2018) 1276–1281, https://doi.org/10.1126/science.aau0630.

[78] A. Kraytsberg, Y. Ein-Eli, Review of advanced materials for proton exchange membrane fuel cells, Energy Fuel. 28 (2014) 7303–7330, https://doi.org/10.1021/ef501977k.

[79] A. Rolfi, C. Oldani, L. Merlo, D. Facchi, R. Ruffo, New perfluorinated ionomer with improved oxygen permeability for application in cathode polymeric electrolyte membrane fuel cell, J. Power Sources 396 (2018) 95–101, https://doi.org/10.1016/j.jpowsour.2018.05.093.

[80] E. Passalacqua, F. Lufrano, G. Squadrito, A. Patti, L. Giorgi, Nafion content in the catalyst layer of polymer electrolyte fuel cells: effects on structure and performance, Electrochim. Acta 46 (2001) 799–805, https://doi.org/10.1016/S0013-4686(00)00679-4.

[81] R.J. Ouimet, T.A. Ebaugh, G. Mirshekari, S. Bliznakov, L.J. Bonville, R. Maric, Current status on the manufacturing of nanomaterials for proton exchange membrane energy systems by vapor-based processes, Energy Fuel. 35 (2021) 1933–1956, https://doi.org/10.1021/acs.energyfuels.0c03670.

[82] I. Fouzaï, S. Gentil, V. Costa Bassetto, W.O. Da Silva, M. Raddaoui, H. Girault, Catalytic layer - membrane electrode assembly methods for optimum formation of triple phase boundaries and fuel cell performances, J. Mater. Chem. 9 (2021) 11096–11123, https://doi.org/10.1039/d0ta07470e.

[83] A. De las Heras, F.J. Vivas, F. Segura, J.M. Andújar, From the cell to the stack. A chronological walk through the techniques to manufacture the PEFCs core, Renew. Sustain. Energy Rev. 96 (2018) 29–45, https://doi.org/10.1016/j.rser.2018.07.036.

[84] K.L. Bhamidipati, S. Didari, T.A.L. Harris, Slot die coating of polybenzimiazole based membranes at the air engulfment limit, J. Power Sources 239 (2013) 382–392, https://doi.org/10.1016/j.jpowsour.2013.03.132.

[85] M. Klingele, M. Breitwieser, R. Zengerle, S. Thiele, Direct deposition of proton exchange membranes enabling high performance hydrogen fuel cells, J. Mater. Chem. 3 (2015) 11239–11245, https://doi.org/10.1039/C5TA01341K.

[86] M.B. Sassin, Y. Garsany, B.D. Gould, K.E. Swider-Lyons, Fabrication method for laboratory-scale high-performance membrane electrode assemblies for fuel cells, Anal. Chem. 89 (2017) 511–518, https://doi.org/10.1021/acs.analchem.6b03005.

[87] R. Maric, UConn developing production method for next-gen PEMFCs, Fuel Cell. Bull. (2012) 15, https://doi.org/10.1016/S1464-2859(12)70115-3, 2012.

[88] X. Ding, J. Liu, T.A.L. Harris, A review of the operating limits in slot die coating processes, AIChE J. 62 (2016) 2508–2524, https://doi.org/10.1002/aic.15268.

[89] T. Steenberg, H.A. Hjuler, C. Terkelsen, M.T.R. Sánchez, L.N. Cleemann, F. C. Krebs, Roll-to-roll coated PBI membranes for high temperature PEM fuel cells, Energy Environ. Sci. 5 (2012) 6076–6080, https://doi.org/10.1039/c2ee02936g.

[90] M. Bodner, H.R. García, T. Steenberg, C. Terkelsen, S.M. Alfaro, G.S. Avcioglu, et al., Enabling industrial production of electrodes by use of slot-die coating for HT-PEM fuel cells, Int. J. Hydrogen Energy 44 (2019) 12793–12801, https://doi.org/10.1016/j.ijhydene.2018.11.091.

[91] M. Stähler, A. Stähler, F. Scheepers, M. Carmo, D. Stolten, A completely slot die coated membrane electrode assembly, Int. J. Hydrogen Energy 44 (2019) 7053–7058, https://doi.org/10.1016/j.ijhydene.2019.02.016.

[92] X. Ding, S. Didari, T.F. Fuller, T.A. Harris, A new fabrication technique to manufacture an MEA using direct coating of Nafion® onto catalyzed GDL, ECS Trans. 33 (2010) 255–265, https://doi.org/10.1149/1.3484523.

[93] X. Ding, S. Didari, T.F. Fuller, T.A.L. Harris, Membrane electrode assembly fabrication process for directly coating catalyzed gas diffusion layers, J. Electrochem. Soc. 159 (2012) B746–B753, https://doi.org/10.1149/2.103206jes.

[94] A. Burdzik, M. Stähler, I. Friedrich, M. Carmo, D. Stolten, Homogeneity analysis of square meter-sized electrodes for PEM electrolysis and PEM fuel cells, J. Coating Technol. Res. 15 (2018) 1423–1432, https://doi.org/10.1007/s11998-018-0074-3.

[95] T.A.L. Harris, D.F. Walczyk, M.M. Weber, Manufacturing of high-temperature polymer electrolyte membranes-Part II: implementation and system model validation, J. Fuel Cell Sci. Technol. 7 (2010), https://doi.org/10.1115/1.3119057, 0110081–8.

[96] T.A.L. Harris, D.F. Walczyk, M.M. Weber, Manufacturing of high-temperature polymer electrolyte membranes-part I: system design and modeling, J. Fuel Cell Sci. Technol. 7 (2010), https://doi.org/10.1115/1.3119055, 0110071–9.

[97] B. Millington, V. Whipple, B.G. Pollet, A novel method for preparing proton exchange membrane fuel cell electrodes by the ultrasonic-spray technique, J. Power Sources 196 (2011) 8500–8508, https://doi.org/10.1016/j.jpowsour.2011.06.024.

[98] S. Kabir, T. Van Cleve, S. Khandavalli, S. Medina, S. Pylypenko, S. Mauger, et al., Toward optimizing electrospun nanofiber fuel cell catalyst layers: microstructure and Pt accessibility, ACS Appl. Energy Mater. (2021), https://doi.org/10.1021/acsaem.0c03073.

[99] H. Yu, J.M. Roller, W.E. Mustain, R. Maric, Influence of the ionomer/carbon ratio for low-Pt loading catalyst layer prepared by reactive spray deposition technology, J. Power Sources 283 (2015) 84–94, https://doi.org/10.1016/j.jpowsour.2015.02.101.

[100] S. Holdcroft, Fuel cell catalyst layers: a polymer science perspective, Chem. Mater. 26 (2014) 381–393, https://doi.org/10.1021/cm401445h.

[101] Y. Liu, C. Ji, W. Gu, J. Jorne, H.A. Gasteiger, Effects of catalyst carbon support on proton conduction and cathode performance in PEM fuel cells, J. Electrochem. Soc. 158 (2011) B614, https://doi.org/10.1149/1.3562945.
[102] H. Yu, A. Baricci, J. Roller, Y. Wang, A. Casalegno, W.E. Mustain, et al., Ultra-low Pt loading catalyst layers for PEMFC using reactive spray deposition technology, ECS Trans. 69 (2015) 487–496, https://doi.org/10.1149/06917.0487ecst.
[103] H.A. Gasteiger, S.S. Kocha, B. Sompalli, F.T. Wagner, Activity benchmarks and requirements for Pt, Pt-alloy, and non-Pt oxygen reduction catalysts for PEMFCs, Appl. Catal. B Environ. 56 (2005) 9–35, https://doi.org/10.1016/j.apcatb.2004.06.021.
[104] H. Yu, A. Baricci, A. Bisello, A. Casalegno, L. Guetaz, L. Bonville, et al., Strategies to mitigate Pt dissolution in low Pt loading proton exchange membrane fuel cell: I. A gradient Pt particle size design, Electrochim. Acta 247 (2017) 1155–1168, https://doi.org/10.1016/j.electacta.2017.07.093.
[105] J.H. Wendorff, S. Agarwal, A. Greiner, Electrospinning: Materials, Processing, and Applications, Wiley-VCH Verlag & Co. KGaA, 2012.
[106] D.H. Reneker, A.L. Yarin, Electrospinning jets and polymer nanofibers, Polymer 49 (2008) 2387–2425, https://doi.org/10.1016/j.polymer.2008.02.002.
[107] S. Cavaliere, S. Subianto, I. Savych, D.J. Jones, J. Rozière, Electrospinning: designed architectures for energy conversion and storage devices, Energy Environ. Sci. 4 (2011) 4761–4785, https://doi.org/10.1039/c1ee02201f.
[108] S. Chan, J. Jankovic, D. Susac, M.S. Saha, M. Tam, H. Yang, et al., Electrospun carbon nanofiber catalyst layers for polymer electrolyte membrane fuel cells: structure and performance, J. Power Sources 392 (2018) 239–250, https://doi.org/10.1016/j.jpowsour.2018.02.001.
[109] Y. Wang, J. Jin, S. Yang, G. Li, J. Qiao, Highly active and stable platinum catalyst supported on porous carbon nanofibers for improved performance of PEMFC, Electrochim. Acta 177 (2015) 181–189, https://doi.org/10.1016/j.electacta.2015.01.134.
[110] J.H. Park, Y.W. Ju, S.H. Park, H.R. Jung, K.S. Yang, W.J. Lee, Effects of electrospun polyacrylonitrile-based carbon nanofibers as catalyst support in PEMFC, J. Appl. Electrochem. 39 (2009) 1229–1236, https://doi.org/10.1007/s10800-009-9787-4.
[111] S. Chan, J. Jankovic, D. Susac, M.S. Saha, M. Tam, H. Yang, et al., Electrospun carbon nanofiber catalyst layers for polymer electrolyte membrane fuel cells: fabrication and optimization, J. Mater. Sci. 53 (2018) 11633–11647, https://doi.org/10.1007/s10853-018-2411-4.
[112] J.B. Ballengee, P.N. Pintauro, Composite fuel cell membranes from dual-nanofiber electrospun mats, Macromolecules 44 (2011) 7307–7314, https://doi.org/10.1021/ma201684j.
[113] J. Choi, R. Wycisk, W. Zhang, P.N. Pintauro, K.M. Lee, P.T. Mather, High conductivity perfluorosulfonic acid nanofiber composite fuel-cell membranes, ChemSusChem 3 (2010) 1245–1248, https://doi.org/10.1002/cssc.201000220.
[114] S. Kotera, H. Watabe, K. Fujii, I. Terada, C. Matsubara, H. Uyama, Study on the cathode fabricated by spinning process and its performance in PEFC, ECS Trans. 25 (2009) 821–830, https://doi.org/10.1149/1.3210635.
[115] K. Waldrop, R. Wycisk, P.N. Pintauro, Application of electrospinning for the fabrication of proton-exchange membrane fuel cell electrodes, Curr. Opin. Electrochem. 21 (2020) 257–264, https://doi.org/10.1016/j.coelec.2020.03.007.
[116] H. Chen, J.D. Snyder, Y.A. Elabd, Electrospinning and solution properties of Nafion and poly(acrylic acid), Macromolecules 41 (2008) 128–135, https://doi.org/10.1021/ma070893g.
[117] W. Zhang, P.N. Pintauro, High-performance nanofiber fuel cell electrodes, ChemSusChem 4 (2011) 1753–1757, https://doi.org/10.1002/cssc.201100245.
[118] M. Brodt, R. Wycisk, P.N. Pintauro, Nanofiber electrodes with low platinum loading for high power hydrogen/air PEM fuel cells, J. Electrochem. Soc. 160 (2013) F744–F749, https://doi.org/10.1149/2.008308jes.
[119] J. Slack, B. Halevi, G. McCool, J. Li, R. Pavlicek, R. Wycisk, et al., Electrospun fiber mat cathode with platinum-group-metal-free catalyst powder and nafion/PVDF binder, Chemelectrochem 5 (2018) 1537–1542, https://doi.org/10.1002/celc.201800283.
[120] M. Brodt, R. Wycisk, N. Dale, P. Pintauro, Power output and durability of electrospun fuel cell fiber cathodes with PVDF and nafion/PVDF binders, J. Electrochem. Soc. 163 (2016) F401–F410, https://doi.org/10.1149/2.0711605jes.
[121] M. Brodt, T. Han, N. Dale, E. Niangar, R. Wycisk, P. Pintauro, Fabrication, in-situ performance, and durability of nanofiber fuel cell electrodes, J. Electrochem. Soc. 162 (2015) F84–91, https://doi.org/10.1149/2.0651501jes.
[122] K. Waldrop, J. Slack, C. Gumeci, N. Dale, K.S. Reeves, D.A. Cullen, et al., Electrospun particle/polymer fiber electrodes with a neat nafion binder for hydrogen/air fuel cells, ECS Trans. 92 (2019) 595–602, https://doi.org/10.1149/09208.0595ecst.
[123] J.J. Slack, C. Gumeci, N. Dale, J. Parrondo, N. Macauley, R. Mukundan, et al., Nanofiber fuel cell MEAs with a PtCo/C cathode, J. Electrochem. Soc. 166 (2019) F3202–F3209, https://doi.org/10.1149/2.0151907jes.
[124] S. Khandavalli, N. Sharma-Nene, S. Kabir, S. Sur, J.P. Rothstein, K.C. Neyerlin, et al., Toward optimizing electrospun nanofiber fuel cell catalyst layers: polymer–particle interactions and spinnability, ACS Appl. Polym. Mater. (2021), https://doi.org/10.1021/acsapm.0c01354.
[125] K.C. Hess, W.K. Epting, S. Litster, Spatially resolved, in situ potential measurements through porous electrodes as applied to fuel cells, Anal. Chem. 83 (2011) 9492–9498, https://doi.org/10.1021/AC202231Y/ASSET/IMAGES/LARGE/AC-2011-02231Y_0004.JPEG.
[126] Z. Xie, T. Navessin, K. Shi, R. Chow, Q. Wang, D. Song, et al., Functionally graded cathode catalyst layers for polymer electrolyte fuel cells: II. Experimental study of the effect of nafion distribution, J. Electrochem. Soc. 152 (2005) A1171, https://doi.org/10.1149/1.1904990.
[127] K.H. Kim, H.J. Kim, K.Y. Lee, J.H. Jang, S.Y. Lee, E. Cho, et al., Effect of Nafion® gradient in dual catalyst layer on proton exchange membrane fuel cell performance, Int. J. Hydrogen Energy 33 (2008) 2783–2789, https://doi.org/10.1016/J.IJHYDENE.2008.03.015.
[128] K.C. Neyerlin, W. Gu, J. Jorne, A. Clark, H.A. Gasteiger, Cathode catalyst utilization for the ORR in a PEMFC: analytical model and experimental validation, J. Electrochem. Soc. 154 (2007) B279, https://doi.org/10.1149/1.2400626.
[129] Q. Wang, M. Eikerling, D. Song, Z. Liu, T. Navessin, Z. Xie, et al., Functionally graded cathode catalyst layers for polymer electrolyte fuel cells: I. Theoretical modeling, J. Electrochem. Soc. 151 (2004) A950, https://doi.org/10.1149/1.1753580.
[130] P.J. Ferreira, G.J. la O', Y. Shao-Horn, D. Morgan, R. Makharia, S. Kocha, et al., Instability of Pt/C electrocatalysts in proton exchange membrane fuel cells, J. Electrochem. Soc. 152 (2005) A2256, https://doi.org/10.1149/1.2050347.
[131] M. Gummalla, S.C. Ball, D.A. Condit, S. Rasouli, K. Yu, P.J. Ferreira, et al., Effect of particle size and operating conditions on Pt3Co PEMFC cathode catalyst durability, Catalysts 5 (2015) 926–948, https://doi.org/10.3390/catal5020926.
[132] L. Dubau, J. Durst, L. Castanheira, F. Maillard, A. Lamibrac, J. Dillet, et al., Various scales of aging heterogeneities upon PEMFC operation - a link between local MEA materials degradation and the cell performance, ECS Trans. 69 (2015) 133–146, https://doi.org/10.1149/06917.0133ecst.
[133] C. Takei, K. Kakinuma, K. Kawashima, K. Tashiro, M. Watanabe, M. Uchida, Load cycle durability of a graphitized carbon black-supported platinum catalyst in polymer electrolyte fuel cell cathodes, J. Power Sources 324 (2016) 729–737, https://doi.org/10.1016/j.jpowsour.2016.05.117.
[134] S. Chen, H.A. Gasteiger, K. Hayakawa, T. Tada, Y. Shao-Horn, Platinum-alloy cathode catalyst degradation in proton exchange membrane fuel cells: nanometer-scale compositional and morphological changes, J. Electrochem. Soc. 157 (2010) A82, https://doi.org/10.1149/1.3258275.
[135] L. Dubau, L. Guetaz, J. Durst, F. Maillard, M. Chatenet, J. Andre, et al., Evidences of "through-plane" heterogeneities of aging in a proton-exchange membrane fuel cell, ECS Electrochem. Lett. 1 (2012) F13, https://doi.org/10.1149/2.011202eel.
[136] H. Nguyen, D. Sultanova, P.A. Heizmann, S. Vierrath, M. Breitwieser, Improving the efficiency of fully hydrocarbon-based proton-exchange membrane fuel cells by ionomer content gradients in cathode catalyst layers, Mat. Adv. 3 (2022) 8460–8468, https://doi.org/10.1039/D2MA00761D.
[137] K.C. Neyerlin, H.A. Gasteiger, C.K. Mittelsteadt, J. Jorne, W. Gu, Effect of relative humidity on oxygen reduction kinetics in a PEMFC, J. Electrochem. Soc. 152 (2005) A1073, https://doi.org/10.1149/1.1897368/XML.
[138] H. Xu, Y. Song, H.R. Kunz, J.M. Fenton, Effect of elevated temperature and reduced relative humidity on ORR kinetics for PEM fuel cells, J. Electrochem. Soc. 152 (2005) A1828, https://doi.org/10.1149/1.1984351/XML.
[139] D. Novitski, S. Holdcroft, Determination of O2 mass transport at the Pt | PFSA ionomer interface under reduced relative humidity, ACS Appl. Mater. Interfaces 7 (2015) 27314–27323, https://doi.org/10.1021/ACSAMI.5B08720/ASSET/IMAGES/LARGE/AM-2015-08720N_0012.JPEG.
[140] H.N. Su, S.J. Liao, Y.N. Wu, Significant improvement in cathode performance for proton exchange membrane fuel cell by a novel double catalyst layer design, J. Power Sources 195 (2010) 3477–3480, https://doi.org/10.1016/J.JPOWSOUR.2009.12.064.
[141] D. Van Dao, G. Adilbish, I.H. Lee, Y.T. Yu, Enhanced electrocatalytic property of Pt/C electrode with double catalyst layers for PEMFC, Int. J. Hydrogen Energy 44 (2019) 24580–24590, https://doi.org/10.1016/J.IJHYDENE.2019.07.156.
[142] J. Ustarroz, B. Geboes, H. Vanrompay, K. Sentosun, S. Bals, T. Breugelmans, et al., Electrodeposition of highly porous Pt nanoparticles studied by quantitative 3D electron tomography: influence of growth mechanisms and potential cycling on the active surface area, ACS Appl. Mater. Interfaces 9 (2017) 16168–16177, https://doi.org/10.1021/ACSAMI.7B01619/ASSET/IMAGES/LARGE/AM-2017-01619Q_0007.JPEG.
[143] J. Kim, J.E. Dick, A.J. Bard, Advanced electrochemistry of individual metal clusters electrodeposited atom by atom to nanometer by nanometer, Acc. Chem. Res. 49 (2016) 2587–2595, https://doi.org/10.1021/ACS.ACCOUNTS.6B00340/ASSET/IMAGES/LARGE/AR-2016-003409_0012.JPEG.
[144] B. Geboes, J. Ustarroz, K. Sentosun, H. Vanrompay, A. Hubin, S. Bals, et al., Electrochemical behavior of electrodeposited nanoporous Pt catalysts for the oxygen reduction reaction, ACS Catal. 6 (2016) 5856–5864, https://doi.org/10.1021/ACSCATAL.6B00668/SUPPL_FILE/CS6B00668_SI_003.MPG.
[145] S.J. Hwang, S.J. Yoo, S. Jang, T.H. Lim, S.A. Hong, S.K. Kim, Ternary Pt-Fe-Co alloy electrocatalysts prepared by electrodeposition: elucidating the roles of Fe and co in the oxygen reduction reaction, J. Phys. Chem. C 115 (2011) 2483–2488, https://doi.org/10.1021/JP106947Q/SUPPL_FILE/JP106947Q_SI_001.PDF.
[146] A. Chavez-Valdez, M.S.P. Shaffer, A.R. Boccaccini, Applications of graphene electrophoretic deposition. A review, J. Phys. Chem. B 117 (2013) 1502–1515, https://doi.org/10.1021/JP3064917/ASSET/IMAGES/MEDIUM/JP-2012-064917_0014.GIF.
[147] A.A. Daryakenari, D. Hosseini, T. Saito, A. Apostoluk, C.R. Müller, J.J. Delaunay, Ethanol electro-oxidation on nanoworm-shaped Pd particles supported by nanographitic layers fabricated by electrophoretic deposition, RSC Adv. 5 (2015) 52578–52587, https://doi.org/10.1039/C5RA06218G.
[148] G. Adilbish, Y.T. Yu, Effect of the Nafion content in the MPL on the catalytic activity of the Pt/C-Nafion electrode prepared by pulsed electrophoresis deposition, Int. J. Hydrogen Energy 42 (2017) 1181–1188, https://doi.org/10.1016/J.IJHYDENE.2016.09.143.

[149] G. Adilbish, J.W. Lee, Y.S. Jang, H.G. Lee, Y.T. Yu, Preparation of Pt/C electrode with double catalyst layers by electrophoresis deposition method for PEMFC, Int. J. Hydrogen Energy 39 (2014) 3381–3386, https://doi.org/10.1016/J.IJHYDENE.2013.11.044.

[150] M. Breitwieser, M. Klingele, B. Britton, S. Holdcroft, R. Zengerle, S. Thiele, Improved Pt-utilization efficiency of low Pt-loading PEM fuel cell electrodes using direct membrane deposition, Electrochem. Commun. 60 (2015) 168–171, https://doi.org/10.1016/J.ELECOM.2015.09.006.

[151] S. Vierrath, M. Breitwieser, M. Klingele, B. Britton, S. Holdcroft, R. Zengerle, et al., The reasons for the high power density of fuel cells fabricated with directly deposited membranes, J. Power Sources 326 (2016) 170–175, https://doi.org/10.1016/J.JPOWSOUR.2016.06.132.

[152] M. Breitwieser, C. Klose, M. Klingele, A. Hartmann, J. Erben, H. Cho, et al., Simple fabrication of 12 μm thin nanocomposite fuel cell membranes by direct electrospinning and printing, J. Power Sources 337 (2017) 137–144, https://doi.org/10.1016/J.JPOWSOUR.2016.10.094.

[153] M. Breitwieser, C. Klose, A. Hartmann, A. Büchler, M. Klingele, S. Vierrath, et al., Cerium oxide decorated polymer nanofibers as effective membrane reinforcement for durable, high-performance fuel cells, Adv. Energy Mater. 7 (2017), 1602100, https://doi.org/10.1002/AENM.201602100.

[154] C. Klose, M. Breitwieser, S. Vierrath, M. Klingele, H. Cho, A. Büchler, et al., Electrospun sulfonated poly(ether ketone) nanofibers as proton conductive reinforcement for durable Nafion composite membranes, J. Power Sources 361 (2017) 237–242, https://doi.org/10.1016/J.JPOWSOUR.2017.06.080.

[155] Y. Zhao, X. Li, W.W. Li, Z. Wang, S. Wang, X. Xie, et al., A high-performance membrane electrode assembly for polymer electrolyte membrane fuel cell with poly(arylene ether sulfone) nanofibers as effective membrane reinforcements, J. Power Sources 444 (2019), 227250, https://doi.org/10.1016/J.JPOWSOUR.2019.227250.

[156] S. Litster, G. McLean, PEM fuel cell electrodes, J. Power Sources 130 (2004) 61–76, https://doi.org/10.1016/j.jpowsour.2003.12.055.

[157] R. O'Hayre, D.M. Barnett, F.B. Prinz, The triple phase boundary: a mathematical model and experimental investigations for fuel cells, J. Electrochem. Soc. 152 (2005) A439, https://doi.org/10.1149/1.1851054.

[158] D. Banham, S. Ye, Current status and future development of catalyst materials and catalyst layers for proton exchange membrane fuel cells: an industrial perspective, ACS Energy Lett. 2 (2017) 629–638, https://doi.org/10.1021/acsenergylett.6b00644.

[159] A. Kongkanand, M.F. Mathias, The priority and challenge of high-power performance of low-platinum proton-exchange membrane fuel cells, J. Phys. Chem. Lett. 7 (2016) 1127–1137, https://doi.org/10.1021/acs.jpclett.6b00216.

[160] I. Falina, A. Pavlets, A. Alekseenko, E. Titskaya, N. Kononenko, Influence of PtCu/C catalysts composition on electrochemical characteristics of polymer electrolyte fuel cell and properties of proton exchange membrane, Catalysts 11 (2021) 1063, https://doi.org/10.3390/catal11091063.

[161] A. Kusoglu, A.Z. Weber, New insights into perfluorinated sulfonic-acid ionomers, Chem. Rev. 117 (2017) 987–1104, https://doi.org/10.1021/acs.chemrev.6b00159.

[162] D.K. Paul, M.A. Hickner, K. Karan, R.A. Segalman, A.Z. Weber, Self-assembly and transport limitations in self-assembly and transport limitations in con fi ned Na fi on films, Macromolecules 46 (2013) 867–873.

[163] O.H. Kim, Y.H. Cho, S.H. Kang, H.Y. Park, M. Kim, J.W. Lim, et al., Ordered macroporous platinum electrode and enhanced mass transfer in fuel cells using inverse opal structure, Nat. Commun. 4 (2013) 1–9, https://doi.org/10.1038/ncomms3473.

[164] Z. Li, S.C. Chang, R.S. Williams, Self-assembly of alkanethiol molecules onto platinum and platinum oxide surfaces, Langmuir 19 (2003) 6744–6749, https://doi.org/10.1021/la034245b.

[165] U.M. Jalal, M. Khalid Hossain, M.I. Hossain, W. Qarony, S. Tayyaba, M.N.H. Mia, et al., Modeling of self-assembled monolayers (SAMs) of Octadecanethiol and Hexadecanethiol on gold (Au) and silver (Ag), Results Phys. 7 (2017) 2289–2295, https://doi.org/10.1016/j.rinp.2017.06.055.